SCIENCE CHINA Materials

REVIEWS

mater.scichina.com link.springer.com

Published online 28 February 2020 | https://doi.org/10.1007/s40843-019-1242-1

Sci China Mater 2020, 63(6): 921–948

SPECIAL TOPIC: Single-atom Catalysts

Electrocatalyst engineering and structure-activity relationship in hydrogen evolution reaction: From nanostructures to single atoms

Yuan Pan[1,2], Chao Zhang[2], Yan Lin[3], Zhi Liu[1], Minmin Wang[1] and Chen Chen[2*]

ABSTRACT **With the ever-pressing issues of global energy demand and environmental pollution, molecular hydrogen has been receiving increasing attention as a clean alternative energy carrier. For hydrogen production, the design and development of high-performance catalysts remains rather challenging. As the compositions and structures of catalyst interfaces have paramount influences on the catalytic performances, the central topic here has always been to design and engineer the interface structures *via* rational routes so as to boost the activities and stabilities of electrocatalysts on hydrogen evolution reaction (HER). Here in this review, we focus on the design and preparation of multi-scale catalysts specifically catering to HER applications. We start from the design and structure-activity relationship of catalytic nanostructures, summarize the research progresses related to HER nanocatalysts, and interpret their high activities from the atomistic perspective; then, we review the studies regarding the design, preparation, HER applications and structure-activity relationship of single-atom site catalysts (SASCs), and thereupon discuss the future directions in designing HER-oriented SASCs. At the end of this review, we present an outlook on the development trends and faced challenges of catalysts for electrochemical HER.**

Keywords: electrocatalyst, structure-activity relationship, hydrogen evolution reaction, nanomaterials, single-atom site catalysts

INTRODUCTION

With the ever-growing global energy demand and ever-pressing environment issues, the concept of "hydrogen economy" has received ever-broadening acknowledgement. Ironically, 95% of the global hydrogen supply now comes (directly or indirectly) from fossil fuels, which, in essence, is in contradiction with the intention of green and sustainable development [1,2]. The water on the Earth constitutes a gigantic reservoir for hydrogen; however, the production of hydrogen from water by electrochemical method is a rather energy-intensive and expensive process, thus not competitive with hydrogen production from fossil fuels. In order to reduce the total energy consumption, the overpotentials in water splitting have to be lowered, and the efficiency has to be elevated [3]. Up to date, relevant catalysts with the highest efficiencies have been Pt and Pt-group metals, which generally suffer from low abundance and high costs, and are therefore unsuitable for large-scale applications in industry [4]. As a result, it has become an urgent task to develop catalysts based on low-cost non-noble metals or single-atom site catalysts (SASCs) featuring low loadings and high activities.

The compositions and structures of surfaces/interfaces of catalysts are known to have great influences on their catalytic performances; one of the central topics in hydrogen evolution reaction (HER) has always been to rationally design and manipulate the chemical compositions, atom arrangement and electronic structures at the catalyst interfaces to boost the activity and stability [5]. Therefore, the key science in catalyst design and preparation is to select the appropriate materials, and

[1] State Key Laboratory of Heavy Oil Processing, China University of Petroleum (East China), Qingdao 266580, China
[2] Department of Chemistry, Tsinghua University, Beijing 100084, China
[3] College of Science, China University of Petroleum (East China), Qingdao 266580, China
[*] Correspondence author (email: cchen@mail.tsinghua.edu.cn)

thereupon to construct specific interface structures and to arrange the surface atoms in optimized configurations. For the preparation methodology of advanced catalysts, scientists need to develop new techniques, including (1) manipulating the nanocatalysts at the atomic level, and (2) fabricating catalytically active single-atom sites.

In this review (Fig. 1), we focus on the multi-scale design and preparation of catalysts for the HER system. We start from the design and structure-activity relationship of catalytic nanostructures, summarize the research progresses related to HER nanocatalysts, and interpret their high activities from the atomistic perspective; then, we review the studies regarding the design, preparation, HER applications and structure-activity relationship of SASCs, and thereupon discuss the future directions in designing HER-oriented SASCs. At the end of this review, we present an outlook on the development trends and faced challenges of electrocatalysts for HER.

NANOCATALYST ENGINEERING FOR HER

Noble metal nanocatalysts

Noble metal Pt is considered as the state-of-the-art HER electrocatalyst for its much lower overpotential at the same current density than those of other materials. However, the large-scale industrial applications of this metal are limited by its low abundance in the Earth's crust. In order to reduce the usages, maximize the atom efficiencies and maintain the high activities, micro-structured, nanostructured even single-atom electrocatalysts with more exposed catalytic atoms have been in pursuit [6,7]. As reported by Chen *et al.* [8], the shape of Pt nanocrystals affects their catalytic activity and selectivity for many electrocatalytic reactions (such as oxygen reduction reaction (ORR), oxidation reaction of methanol, ethanol, and formic acid), but for HER the activity is mainly mentioned under the general test conditions. Li *et al.* [9] reported an under-water, super-

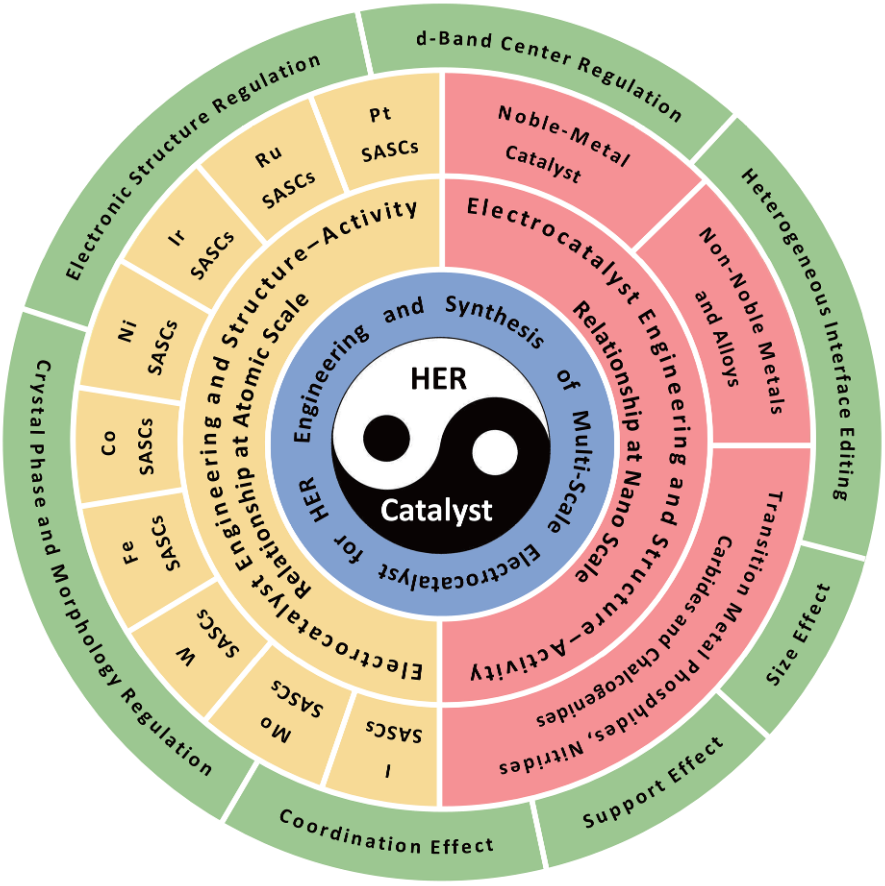

Figure 1 The summarized schematic illustration of the research routes in this review.

aerophobic, nanostructured Pt electrode with a pine-like shape, which shows much better electrocatalytic HER performances, with a dramatically abrupt increase in current density with overpotential (3.85 mA mV^{-1}), which is 2.55 and 13.75 times higher than that of Pt nanospheres and Pt flat electrodes. Introducing carbon materials is an effective way to design various novel Pt-based nanocatalysts for HER. Bai *et al.* [10] prepared a unique Pd@Pt/graphene hybrid structure with Pt shell thickness tunable (0.8–3.2 nm) (Fig. 2a–c). The results suggest the Pt shell thickness greatly affects the HER performance. When the shell thickness is reduced to 0.8 nm, the highest HER performance can be achieved (791 mA cm^{-2} at 300 mV, Tafel slope of 10 mV dec^{-1}) (Fig. 2d and e). The team proposed a surface polarization mechanism, by which the shell thickness can be minimized, thus reducing the usage of Pt.

Another effective way is reducing the Pt loadings while better utilizing its high activity by combining other earth-abundant elements. Esposito *et al.* [11] selected "Pt-like" transition metal carbides (such as tungsten carbides, WCs) to support the lowest possible loading (monolayer) of Pt. Their studies suggest that replacing Pt atoms with WC would not compromise the electrocatalytic activity, and can also reduce the Pt loading in various electrocatalytic applications by over an order of magnitude. They also tried to support one Pt monolayer on molybdenum carbide (Mo_2C) to reduce the cost. The results suggest that this catalyst shows a Pt-like activity and excellent stability under HER conditions. Xing *et al.* [12] used a three-dimensional (3D) substrate (carbon cloth supported $Co(OH)_2$ nanosheet (NS) array ($Co(OH)_2$/CC)) for Pt electrodeposition, and obtained a sample denoted as Pt-$Co(OH)_2$/CC (with 5.7 wt% Pt loading). It showed top performances for HER in both alkaline and neutral conditions (4.8 and 2.6 times higher than those of commercial Pt/C/CC, respectively). The synergistic catalytic effects between $Co(OH)_2$ and Pt at the nano-interfaces led to the greatly improved performances. Similarly, Xie *et al.* [13] directly grew an ultralow-Pt-content (5.1 wt%) $Ni(OH)_2$-PtO_2 hybrid NS array on Ti mesh (the resulting product denoted as $Ni(OH)_2$-PtO_2 NS/Ti). It exhibits a superior activity (31.4 mV at 4 mA cm^{-2}) in 0.1 mol L^{-1} KOH. This catalyst also shows an excellent stability, with nearly 100% faradaic efficiency after at least 100 h. Density functional theory (DFT) calculations reveal that the interface formed between $Ni(OH)_2$ and PtO_2 greatly promotes the H_2O dissociation kinetics and optimizes the hydrogen adsorption free energy, thus boosting the HER process. Tiwari *et al.* [14] used melamine-derived graphitic tubes (GTs) to anchor a multi-component catalyst with ultralow Pt loading (1.4 μg/electrode area (cm^2)). With a Pt loading only 1/80 of that for commercial 20% Pt/C, this catalyst only needs 18 mV to deliver 10 mA cm^{-2} in 0.5 mol L^{-1} H_2SO_4, and gives a turnover frequency (TOF) 96 times higher (7.22 s^{-1}) than that for Pt/C catalyst, and it also shows a long-term durability (for 10,000 cycles).

Downsizing Pt nanoparticles (NPs) to clusters or even single atoms can maximize the exposure of active sites and then greatly reduce the usage, which is desirable for Pt-related industrial applications [15]. Wang *et al.* [16] designed ultrafine Pt nanoclusters (NCs) confined by a trigonal prismatic coordination cage (Fig. 2f–h). The HER electrocatalytic activity of the Pt NCs is higher than that of commercial Pt/C (Fig. 2i and j) owing to the highly active surface, as well as the synergism between Pt NCs and cage matrix. Besides, downsizing Pt to single-atom scale can maximize the atom utilization by exposing nearly all the metal atoms as active sites, which will be discussed later (vide infra). Alloying Pt-group metals with other non-noble metals (such as Cu [17,18], Fe [19], Co [20,21]) can also be used to lower the loading. Previous studies have suggested that metal Ni possesses a moderate hydrogen binding energy close to that of Pt, and Pt-Ni alloy may thus exhibit profitable electronic and synergistic effect for HER. Solvothermal method has been proved competent for the preparation of Pt-Ni alloys. Hexagonal close-packed Pt-Ni alloy nano-multipods were prepared through a facile one-pot solvothermal method by Cao *et al.* [5]. This Pt-Ni nano-multipods show superior HER catalytic performance in alkaline condition (65 mV at 10 mA cm^{-2}, mass current density is 3.03 mA $mg(Pt)^{-1}$ at −70 mV) thanks to the unique crystal structure and excavated polyhedral morphology. Zhang *et al.* [21] also prepared Pt-Ni anisotropic superstructures (Pt-Ni ASs) through a solvothermal method, which showed spatial heterogeneity (Fig. 2k–m). Fourier transforms of EXAFS spectra of Pt L3-edge and Ni K-edge demonstrated the formation of Pt-Ni ASs (Fig. 2n and o). The HER electrocatalytic performances (27.7 mV at 10 mA cm^{-2}, with TOF reaching 18.63 H_2 s^{-1} at 50 mV) of these Pt-Ni ASs in alkaline conditions are superior to that for commercial Pt/C (Fig. 2p and q). Oh *et al.* [22] prepared hexapod-shaped Pt-Ni-Co alloy nanocatalysts for the efficient alkaline HER through the selective removal of the Ni@Co shell from core@double-shell Pt@Ni@Co nanostructures. Studies suggest Co precursor greatly affects the size and shape of this nanostructure. This Pt-Ni-Co catalyst shows a 10 times higher specific

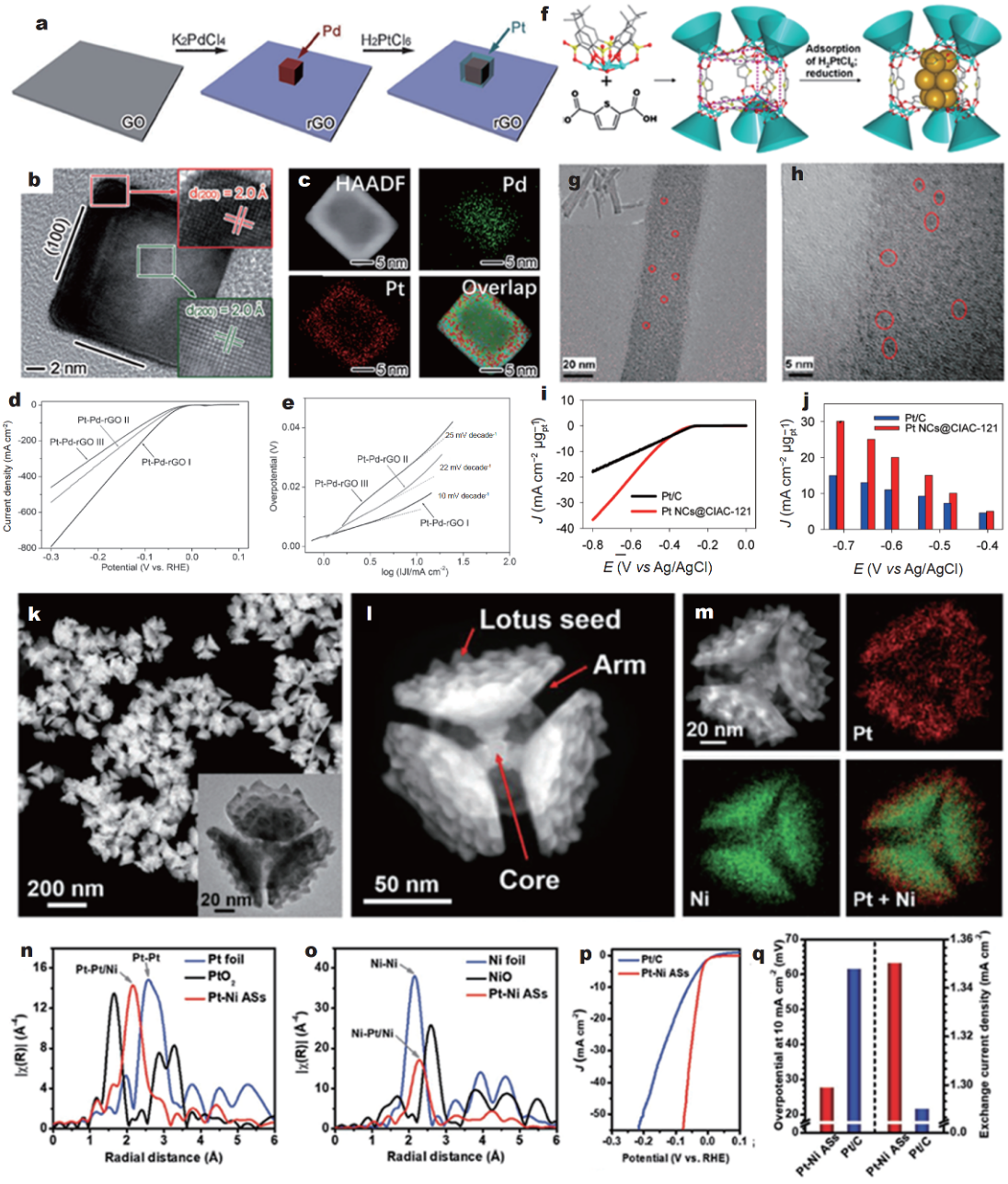

Figure 2 (a) Schematic illustration, (b) high resolution transmission electron microscopy (HRTEM), and (c) high-angle annular dark-field scanning transmission electron microscopy (HAADF-STEM) and energy dispersive spectroscopy (EDS) mapping images of Pt-Pd nanocrystal on reduced graphene oxide (rGO). (d) Linear sweep voltammetry (LSV) curves and (e) Tafel plots of Pt-Pd-rGO structures with different Pt thicknesses. The dashed lines in (e) indicate the linear regions. Adapted with permission from Ref. [10]. Copyright 2014, Wiley-VCH Verlag GmbH & Co. (f) Illustration of the assembly of trigonal prismatic $\{Ni_{24}\}$ coordination cage and the fabrication of ultrafine Pt NCs. (g, h) Transmission electron microscopy (TEM) of the Pt@CIAC-121 hybrids at different magnifications. (i) LSV curves of the Pt@CIAC-121 and Pt/C in 0.5 mol L^{-1} H_2SO_4 for HER. (j) Comparison of current densities between Pt@CIAC-121 and Pt/C at different potentials. Adapted with permission from Ref. [16]. Copyright 2016, the American Chemical Society. (k, l) HAADF-STEM images of the Pt-Ni anisotropic superstructures (ASs). Inset in (k): TEM image of a single Pt-Ni AS. (m) HAADF-STEM and EDS elemental mapping images of a typical Pt-Ni AS. (n) Fourier transforms of extended X-ray absorption fine structure (EXAFS) spectra at Pt L3-edge. (o) Fourier transforms of EXAFS spectra of Ni K-edge. (p) LSV curves of Pt-Ni ASs and Pt/C in 1.0 mol L^{-1} KOH. (q) Overpotentials at current density of 10 mA cm^{-2} (left) and exchange current densities (right) of Pt-Ni ASs and Pt/C. Adapted with permission from Ref. [21]. Copyright 2018, Wiley-VCH Verlag GmbH & Co.

activity than that of Pt/C. Shen *et al.* [23] prepared carbon nanofiber (CNF) arrays decorated with Pt-Cu-Ni NPs, which were conformally assembled on carbon felt (CF) (denoted as PtCuNi/CNF@CF) through an ambient-pressure chemical vapor deposition (CVD) process followed by a spontaneous galvanic replacement reaction. This PtCuNi/CNF@CF is proved to be an ideal binder-free HER eletrocatalyst on account of the high porosity, well-defined geometry shape, good electron conductivity, and particular characteristic of PtCuNi NPs in the tips of CFs.

Non-noble metals and related alloys

Ni has a moderate hydrogen binding energy, but metallic Ni itself is not an ideal HER catalyst. Ni-Fe, Ni-Co, Ni-Mo, Ni-Zn, Ni-W and Ni-Cr alloys have been explored for HER, and among them NiMo alloy is the most promising candidate, yet it still has difficulty to match with Pt in both activity and stability [24]. Besides alloying, hybridizing with carbon materials has also been proved to be an efficient way to boost the HER performances of transition metals. Deng *et al.* [25] reported nitrogen-doped carbon nanotubes (NCNTs) encapsulated Fe, Co and the FeCo alloy (Fig. 3a) for HER in acid. The optimized catalysts exhibited a good HER catalytic performance (onset overpotential is 70 mV), which was close to that of 40% Pt/C catalyst (Fig. 3b). DFT calculations indicated that the optimized electronic structure and the moderate adsorption free energy of H atoms on the catalyst's surface promoted the HER process (Fig. 3c and d). Motivated by these results, they also encapsulated a uniform CoNi nanoalloy by ultrathin (1–3 layers) graphene shells (Fig. 3e–g). The optimized catalyst exhibits almost zero onset overpotential, and needs 142 mV to deliver 10 mA cm^{-2} (Fig. 4h), which is comparable to that of commercial 40% Pt/C [26]. DFT results show that the high HER activity can be attributed to the moderate free energy of H adsorption and the electronic potential distribution at the graphene surface (Fig. 3i and j). Additionally, the decrease of the graphene layer number and the increase of nitrogen dopant amount can improve the electron density of the graphene shells, enhancing the HER electrocatalytic performance (Fig. 3k). Tavakkoli *et al.* [27] decorated single-walled carbon nanotubes (SWNTs) with novel single-shell carbon-encapsulated Fe NPs (SCEINs) (Fig. 3l–m). The single carbon layer in SCEIN/SWNT would not prevent the desired contact between the reactants and vicinity of the Fe NPs, but can protect the active Fe core from oxidation. Thus, this SCEIN/SWNT displays superior HER catalytic properties (onset potential is about 0 V, Tafel slope is 40 mV dec^{-1}), which are even comparable to those of Pt in 0.5 mol L^{-1} H_2SO_4 (Fig. 3n).

Transition metal compounds

Because the HER process occurs on the surface of the electrocatalysts, and the surface adsorption for hydrogen is an important step, the Gibbs free energy of hydrogen adsorption (ΔG_{H^*}) can work as an indicator to predict whether a certain material is ideally capable of catalyzing HER. When ΔG_{H^*} has a large negative value, it suggests that the affinity between H_{ads} and the catalyst surface is too strong, and it is difficult for the formed H_{ads} occupying the active site to desorb, decreasing the catalytic activity. When ΔG_{H^*} has a large positive value, it suggests that H_{ads} and the catalyst surface have a weak binding, which is not conducive to the formation of H_{ads} and transition state of hydrogen, also decreasing the catalytic activity. Therefore, an ideal ΔG_{H^*} for HER should be close to 0. Nørskov *et al.* [28] obtained a volcano-like curve by plotting ΔG_{H^*} *versus* the exchange current density. The higher exchange current density suggests the better catalytic activity of the catalyst. Noble metals, such as Pt, located at the top of the volcano with ΔG_{H^*} close to 0, are expected to have the best catalytic activity. Besides, transition metals Ni, Fe, Co, Cu, Mo, and W also have appropriate ΔG_{H^*} values, and can form borides, carbides, nitrides, chalcogenides and phosphides as efficient HER electrocatalysts [6].

Transition metal phosphides

In 2005, Liu *et al.* [29] used DFT calculation to investigate the Ni_2P (001) surface, and their studies suggest that the introduced P dilutes the surface concentration of Ni and avoids the inactivation of active sites caused by strong surface adsorption of H atoms. Besides, the formation of the Ni–P bonds disturbs the electronic states of the initial Ni, exhibiting a [NiFe] hydrogenase-like electronic structure. Thus, Ni_2P was inferred to be a highly active HER electrocatalyst. However, it was not until 2013 that this inference was verified by Schaak's group [30], and in the same year, Zhang's group [31] first reported that FeP was efficient on HER. Since then, the application of transition metal phosphides in HER began to develop [32,33]. In 2018, with core-shell ZIF-8@ZIF-67 as the precursor, Pan *et al.* [34] designed and synthesized a novel hybrid nanocatalyst—N-doped carbon nanotube hollow polyhedron (NCNHP) encapsulated CoP NPs by a pyrolysis-oxidation-phosphidation strategy (Fig. 4a–c). During the pyrolysis process, ZIF-8 worked as seed, the Zn nodes can evaporate at high temperature, and uni-

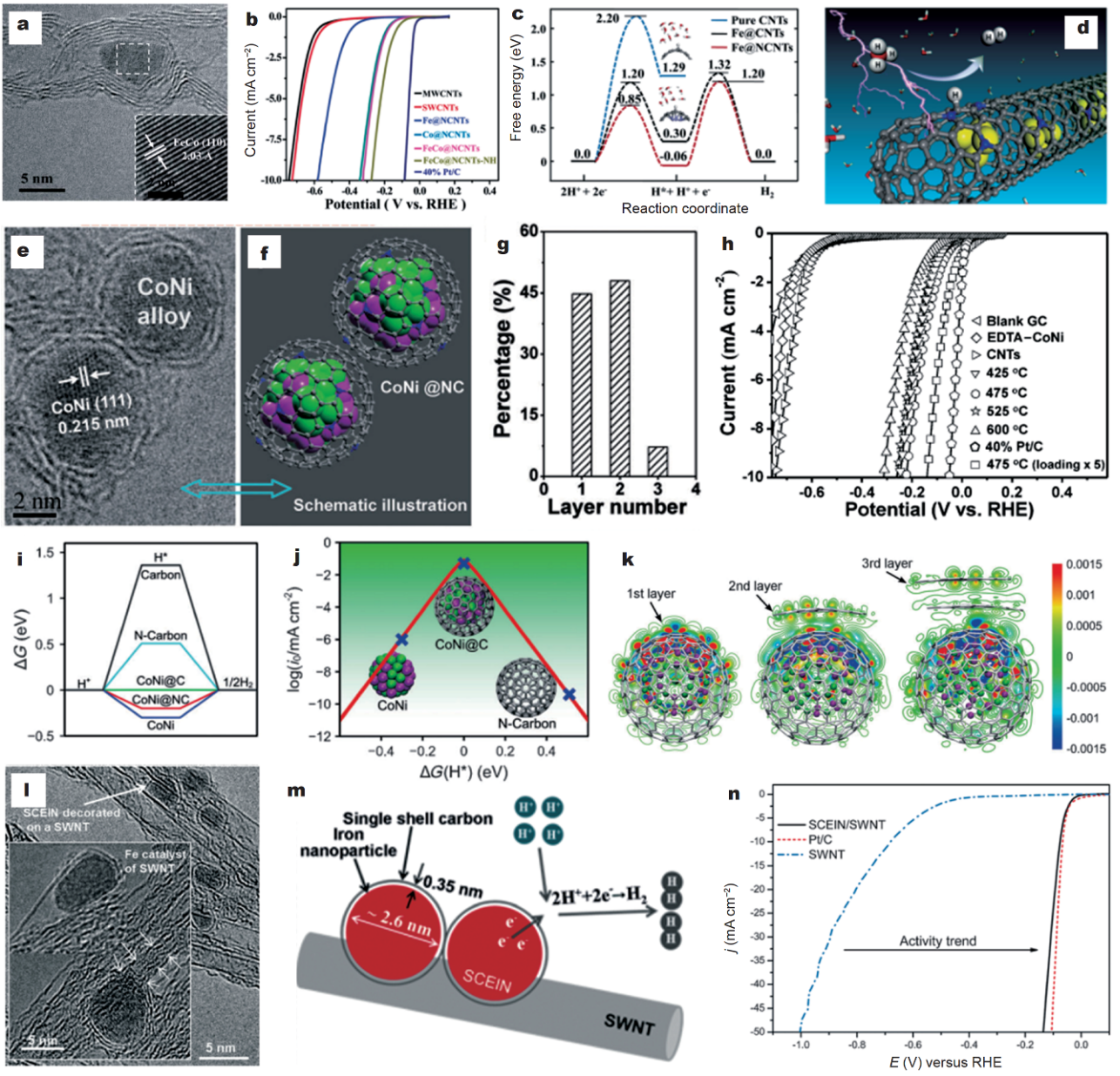

Figure 3 (a) HRTEM image of FeCo@NCNTs with the inset showing the (110) crystal plane of the FeCo nanoparticle. (b) LSV curves. (c) The free energy profiles of the Heyrovsky route. (d) A schematic representation of the HER process on the surface of Fe@NCNTs. The gray balls represent C atoms, yellow for Fe, blue for N, red for O and white for H. Reproduced with permission from Ref. [25]. Copyright 2014, the Royal Society of Chemistry. (e) HRTEM image of CoNi@NC, showing the graphene shells and encapsulated metal NPs. Inset (e): crystal (111) plane of the CoNi alloy. (f) Schematic illustration of the CoNi@NC structure shown in (e). (g) Statistical analysis of the number of layers in the graphene shells encapsulating the metal NPs in CoNi@NC. (h) HER LSV curves for CoNi@NC samples prepared at different temperatures. (i) Gibbs free energy (ΔG) profile of the HER on various catalysts. (j) Volcano plot of the polarized current (i_0) *versus* ΔG_{H^*} for a CoNi cluster, CoNi@C, and an N-doped graphene shell (N-carbon). (k) Redistribution of the electron densities after the CoNi clusters have been covered by 1–3 layers of graphene. The differential charge density is defined as the difference in the electron density with and without the CoNi cluster. The red and blue regions are regions of increased and decreased electron density, respectively. Adapted with permission from Ref. [26]. Copyright 2015, Wiley-VCH Verlag GmbH & Co. (l) HRTEM image of SCEINs decorated on the sidewalls of the SWNTs; the inset shows Fe catalyst particles for the growth of the SWNTs (arrows demonstrate the SWNT). (m) Schematic representation of SCEIN/SWNT sample simplifying the HRTEM images and HER on SCEINs. (n) The polarization curves of SWNT (blue), SCEIN/SWNT (black), and Pt/C (red). The LSV curves were measured at a scan rate of 50 mV s^{-1} in 0.5 mol L^{-1} H_2SO_4. Adapted with permission from Ref. [27]. Copyright 2015, Wiley-VCH Verlag GmbH & Co.

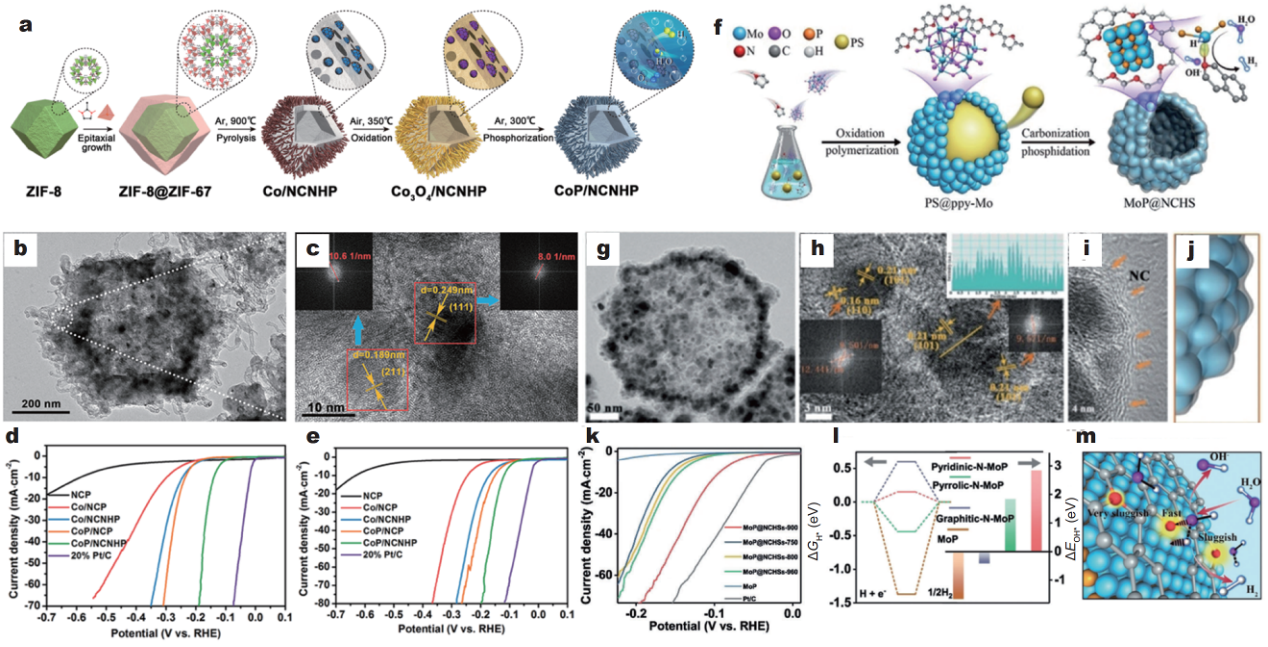

Figure 4 (a) Schematic illustration and (b, c) TEM and HRTEM of the CoP/NCNHP catalyst. Inset in (c): fast Fourier transform (FFT) of the selected area in the red box. (d, e) LSV of CoP/NCNHP and the compared samples in 0.5 mol L^{-1} H_2SO_4, and 1 mol L^{-1} KOH for HER, respectively. Adapted with permission from Ref. [34]. Copyright 2018, the American Chemical Society. (f) Schematic illustration, (g–i) TEM and HRTEM images of MoP@NCHSs-900. Insets in (h): the intensity profile along the yellow line, the FFT of the selected area of orange arrows. (j) Structural model of (i). (k) LSV curves of electrocatalysts MoP@NCHSs-T, bulk MoP, and commercial 20% Pt/C in 1.0 mol L^{-1} KOH. (l) ΔG_{H^*} diagram (left) and the chemisorption energies of OH^* (ΔE_{OH^*}) (right). (m) The schematic of the charge density differences, average Bader charge of NC and water dissociation ability for three N forms based on the DFT calculation results. Blue, orange, red, silver, purple, and white balls represent Mo, P, N, C, O, and H atoms, respectively. Adapted with permission from Ref. [35]. Copyright 2019, Wiley-VCH Verlag GmbH & Co.

formly dispersed Co NPs formed in the pyrolysis process of ZIF-67 shell. Besides, they found the evaporation of the Zn favorable for the formation of CNTs, then the mass transfer was promoted. Due to the strong synergy between the CoP NPs and NCNHP, CoP/NCNHP shows high HER (in acid and alkali) and oxygen evolution reaction (OER) performance (in alkali) (Fig. 4d and e). Given to the good electrocatalytic performance, they assembled a primary battery with this catalyst, the electrocatalytic measurement suggests the full water electrolysis can be driven at 1.64 V, and shows excellent stability (36 h without almost no attenuation of activity). DFT calculation suggests the electron transfer from NCNHP to CoP NPs can effectively increase the d-orbital density near Fermi level of Co, promoting the adsorption of hydrogen and improving the electrocatalytic performance. Meanwhile, the theoretical calculation also suggests the high oxidation resistance of the CoP/NCNHP greatly improves the stability. This work is of great significance for the design and application of transition metal phosphides/carbon based catalysts with high efficiency, stability and novel structure. In 2019, in research of Zhao *et al.* [35], polystyrene (PS) spheres was used as sacrificial templates, and $H_3PMo_{12}O_{40}{\cdot}nH_2O$ was used as oxidant to initiate pyrrole (Py) monomers around PS templates to polymerize. After pyrolysis, MoP NPs were successfully encapsulated in nitrogen-doped carbon hollow spheres to form the core-shell structure of HER electrocatalyst (MoP@NCHSs) (Fig. 4f–j). This catalyst shows good HER electrocatalytic performance, it only needs 92 mV to achieve the current density of 10 mA cm^{-2} (Fig. 4k). And the studies suggest that the synergistic effect between MoP and pyridine N effectively promotes the alkaline HER process, and the interaction between them greatly increases the electron density on the NCHSs carrier, thus accelerating HER; besides these, the d-band center of Mo atom at the interface between pyridine N and MoP decreases, weakening the Mo–H_{ads} bond, and inhibiting the strong adsorption of OH^* by pyridine N (Fig. 4l and m).

The theoretical calculation results suggest that P in transition metal phosphides plays a key role in the HER process. On the one hand, the electronegative P atoms in phosphides can attract electrons transferred from metals,

making the P atoms negatively charged and the metal atoms positively charged. The P with negative charge not only works as an alkaline group to trap the protons produced in the process of hydrogen precipitation, but also promotes the dissociation of hydrogen, thus avoiding the long-time occupation of the active sites owing to the strong adsorption of hydrogen. Wang's group [36] gave an elaboration on the effect of P on the hydrogen evolution. Their study suggests that the P atoms in MoP can work as "hydrogen deliverers", and P can bond with hydrogen at low coverages but release hydrogen at high coverages. The special function of P atoms can create rich active sites in MoP, making the phosphides very suitable for HER. Besides, P atoms can also improve the corrosion resistance of phosphides especially in acid. The undesired dissolution becomes thermodynamically unfavorable because of the P atoms. At the same time, the surface oxidation to form phosphate can further protect the phosphides from dissolution in the electrolyte. Generally, increasing the atomic percentage of P can produce more HER active sites and improve the stability of the phosphides. However, the delocalization of electrons on the metal is greatly limited by the highly electronegative P atoms, impairing the electrical conductivity. Thus, it is important to balance these two aspects by adjusting the atomic ratio of P and the metal.

Recently, some research results [37,38] suggest there exists only one kind of electron transfer in single metal phosphides, producing only one kind of active sites, which is not efficient enough for HER. Introducing a foreign metal can provide more kinds of electron transfer, and produce more active sites; also, there may exist synergistic and complementary effect between different atoms, thus bi-metallic and even multi-metallic phosphides usually show better HER electrocatalytic performances with respect to single-metallic counterparts. Tang *et al.* [39] developed ternary $Fe_xCo_{1-x}P$ nanowire array on carbon cloth ($FexCo_{1-x}P$/CC) for electrocatalytic HER. Their studies suggest that the amount of Fe strongly affect the HER activity. Electrocatalytic test suggests that $Fe_{0.5}Co_{0.5}P$/CC has the best activity (37 mV at 10 mA cm^{-2}). DFT calculations suggest that the replacement of Co by Fe in CoP optimizes ΔG_{H^*} on the catalyst surface. Similarly, the study of Li *et al.* [40] suggests that a proper doping ratio of Fe in Ni_2P can also significantly improve the HER performance. The research of Liang *et al.* [41] also suggests that the HER electroactivity of MoP can be remarkably enhanced by the proper introduction of Fe. Li *et al.* [42] synthesized rGO incorporating Co-doped nickel phosphides ($Ni_{2-x}Co_xP$). The doping of Co and the hybridization with rGO effectively improve the HER electrocatalytic performance within the pH range of 0–14, by virtue of the enriched active sites on the catalyst surface and the accelerated charge transfer. DFT calculations suggest the Co doping leads to the moderate adsorption of atomic hydrogen and easy desorption of the formed H_2. Man *et al.* [43] prepared Ni_2P NPs doped with transition metals (Fe, Co, Mn and Mo) for electrocatalytic HER. Their results suggest that Mo-doped Ni_2P shows the best HER electrocatalytic activity because of the largest degree of d-electron delocalization.

Transition metal sulfides

Hydrodesulfurization (HDS) proceeds *via* a similar pathway to that of HER, both including a reversible surface adsorption/desorption of hydrogen, thus broadening the scope of the search for new HER catalysts. Sulfides, especially MoS_2, are widely used as HDS catalysts to remove sulfur from natural gas and fuels, and have proved to be efficient HER electrocatalysts [44]. Fe [45], Co [46–48], Ni [49] and W [50–53] could also form sulfides that are applicable to HER.

As early as 1977, Tributsch *et al.* [54] suggested that bulk natural crystals of MoS_2 might show HER electrocatalytic activity, yet its potential as efficient HER electrocatalyst was not fully unveiled until 20 years later. In 2005, Hinnemann *et al.* [55] suggested that the basal plane of MoS_2 is catalytically inert, while the true active species are the sulfidated Mo-edges, on the basis of analyzing the free energy of hydrogen using DFT calculations. Two years later, this inference was proved experimentally by Jaramillo *et al.* [56]. Now, this notion has been widely accepted among the researchers. Therefore, subsequent efforts have been devoted to maximizing the exposure of such edge sites, among which one efficient strategy is nano-structuring [57]. Kong *et al.* [58] maximized the exposure of edges by growing MoS_2 and $MoSe_2$ thin films with vertically aligned layers. Their studies suggest that through this kinetically controlled rapid growth strategy, the edge-terminated structure can be synthesized on a diverse range of substrates. Kibsgaard *et al.* [59] engineered the MoS_2 surface structure which preferentially expose the edge sites by fabricating contiguous large-area thin films of a highly ordered double-gyroid MoS_2 bicontinuous network with nanosized pores. The high surface curvature of this mesostructure of the catalyst helps to expose a large fraction of edge sites and provide high surface area, leading to an excellent HER electrocatalytic activity. Wang *et al.* [60] used selective steam etching to improve the density of active edge sites

on MoS_2 basal plane. They suggest that the temperature greatly affects the etched structure, and MoS_2 basal planes with 1D nano-channels, 2D in-plane triangular pits and 3D vertical hexagonal cavities can be created by increasing the temperature. The studies indicate that the surface free energy barrier can be effectively decreased by the extensive created active edges existing on the MoS_2 basal plane, thus improving the HER electrocatalytic activity.

Recently, a pioneering strategy of introducing S vacancies into the basal plane has been proposed, which can also improve the electrocatalytic performance. Li *et al.* [61] firstly introduced S vacancies and strain activated to activate and optimize the basal plane of monolayer 2H-MoS. Their results show that creating and straining S vacancies in the basal plane is efficient for optimizing the electronic structure of MoS_2 to enhance the HER activity. New bands in the gap near the Fermi level can be produced by S vacancies, and these states are localized around the S vacancies, and hydrogen adsorption takes place on these new gap states. With more S vacancies, the number of gap states increases and the bands shift towards the Fermi level. In addition, introducing tensile strain makes the positions of these new bands further move towards the Fermi level, which narrows the band gap and increases the number of gap states around the Fermi level, leading to the increased adsorption strength on S vacancy site. Later, the HER kinetic data for both unstrained and strained S vacancies on the basal plane of MoS_2 monolayers were studied through scanning electrochemical microscopy. Their study suggests that the strained S vacancy has a 4 times higher electron-transfer rate than that of the unstrained S vacancy. Besides, about 2% uniaxial tensile strain increases almost four folds the electron-transfer rate constant (k_{sv}^{0}=1.0×10^{-3} cm s^{-1}), confirming that the HER kinetics of S vacancies in MoS_2 indeed can be accelerated by tensile elastic strain [62]. Tsai *et al.* [63] introduced electrochemical desulfurization to generate S vacancies on the MoS_2 basal plane. In the electrochemical desulfurization process, the S atoms in the basal plane are hydrogenated into H_2S and then removed to form the S vacancies. The HER activity can be significantly improved by varying the extent of desulfurization and the concentration of S vacancies due to the changed applied desulfurization potential and duration. Li *et al.* [64] reported the grain boundary may also provide some catalytic activity for HER. Zhu *et al.* [65] reported that domain boundaries in the basal plane of monolayer MoS_2 can act as active sites for HER. Their studies suggest the multi-hierarchy design on the 2H-2H domain boundaries and 2H-1T phase boundaries can greatly improve the HER performances (activity, stability and universality in both acid and alkali).

Transition metal selenides

Se locates in the same main group as S does in the periodic table; therefore, metal selenides may possess great potential for HER as well. In 2012, NiSe was prepared for HER by Gao *et al.* [66]. Zhou *et al.* [67] demonstrated that commercial Ni foam can be used as the starting material to fabricate a robust porous $NiSe_2$ electrocatalyst by simple acetic acid treatment and thermal selenization in Ar atmosphere. X-ray photoelectron spectroscopy (XPS) and EDS analysis suggest that a small fraction of elemental Se is detected on the surface, and theoretical calculations suggest the adsorbed Se monomers or dimers on the surface could optimize ΔG_{H^*}. Facilitated by the large electrochemically active surface and good electrical conductivity, this $NiSe_2$ exhibits good catalytic activity that approaches that of the benchmark Pt. Kong *et al.* [68] developed $CoSe_2$ NPs grown on carbon fiber paper, which exhibit an excellent HER activity (~180 mV at 100 mA cm^{-2}, Tafel slope is ~40 mV dec^{-1}). Studies on molybdenum selenide ($MoSe_2$) and tungsten selenide (WSe_2) as HER catalysts are not as extensive as those on $MoSe_2$ and WSe_2. Through periodic DFT, Tsai *et al.* [69] studied the structures of the Mo/W-edges and the Se-edges under HER conditions and their differential hydrogen adsorption free energies. Mo-edge and Se-edge on both $MoSe_2$ and WSe_2 are found to be the predominant active facets, and are predicted to have HER activities comparable or even superior to that of MoS_2. The design optimization for $MoSe_2$ and WSe_2, which could maximize the exposure of edge sites, are also efficient for improving HER performances. Coupling with highly conductive carbon materials can help to expose more active sites and accelerate the electron transfer process. Liu *et al.* [70] synthesized $MoSe_2$ nanostructures anchored on rGO NSs ($MoSe_2$/rGO) for HER. The rich defects in the $MoSe_2$ layers and high electrical conductivity of rGO are in favour of the exposure of active edge sites and electron transfer, leading to the excellent HER performance. Tang *et al.* [71] prepared $MoSe_2$ NSs and $MoSe_2$/graphene hybrids for HER. Both the experimental and theoretical studies indicate that $MoSe_2$ has a great potential for HER, and even may exceed MoS_2. Yin *et al.* [72] simultaneously regulated the phase and disorder to maximize the HER activity of $MoSe_2$. The synthesized, partially crystallized 1T-$MoSe_2$ NSs show an excellent HER performance. Through structural and defect characterizations, they concluded that the synergistic regulations of both phase

and disorder in this 1T-$MoSe_2$ NSs facilitated the HER process.

Transition metal carbides

Carbides (such as vanadium carbide [73], nickel carbide [74], niobium carbide [75] and tantalum carbide [75]) have been reported for efficient electrocatalytic HER, and molybdenum carbide and tungsten carbide are two typical examples. As early as 1970s, the studies of Levy [76] and Bennett [77] suggested that introducing carbon to tungsten (named tungsten carbide) can make the electronic density of states (DOS) more resemble that of Pt near the Fermi level, and tungsten carbide therefore should have potential for HER. To some extent, substantially reducing the particle sizes to nanoclusters or even single atoms, would be effective to obtain a high HER activity. Xu *et al.* [78] synthesized ultrasmall tungsten carbide nanoclusters/NPs to achieve the ultrahigh catalytic activities (Fig. 5a–c). They selected an RHO-type zeolitic metal azolate framework MAF-6 with large na-

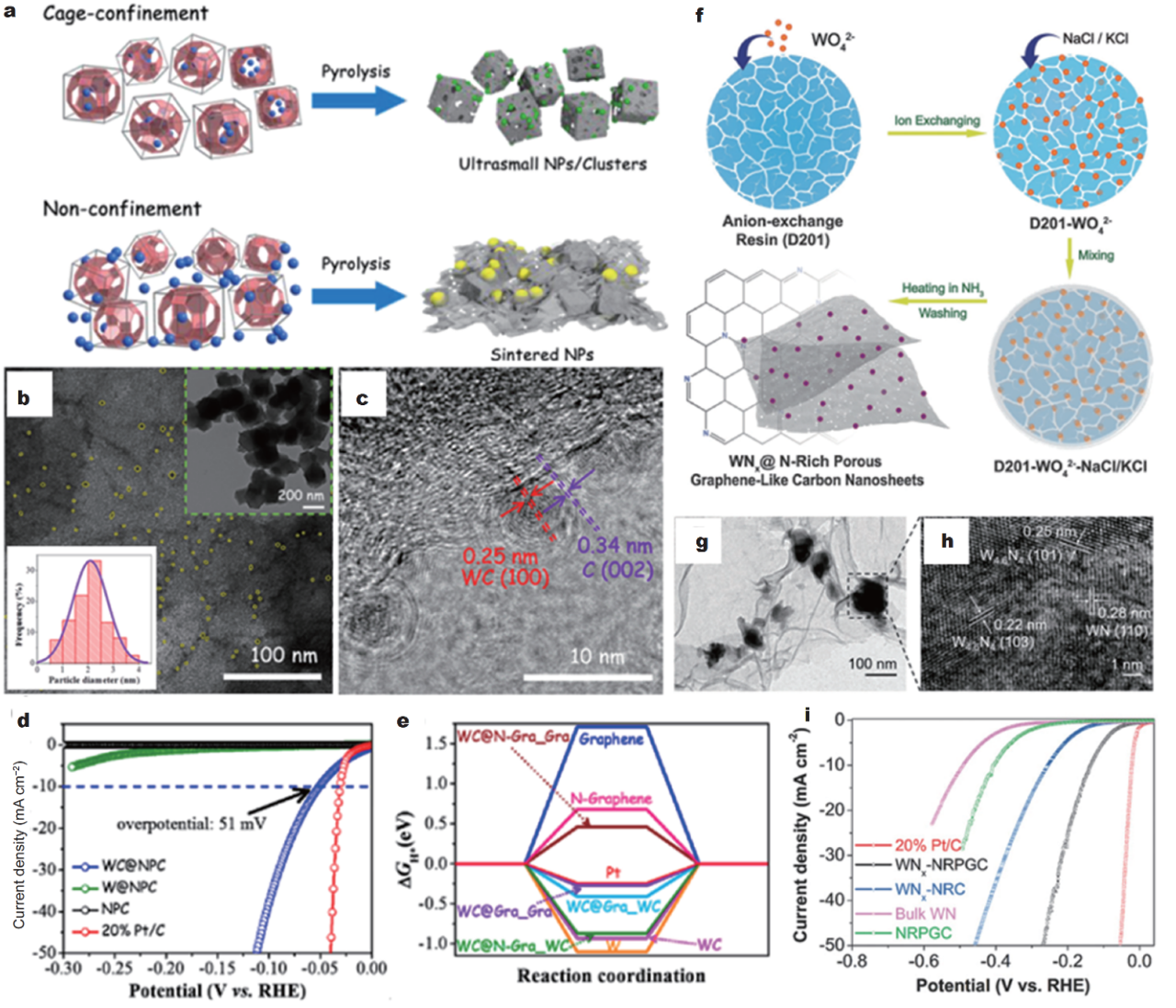

Figure 5 (a) Comparison between the cage-confinement and non-confinement pyrolysis methods for synthesizing nanocatalysts. (b) TEM, (c) HRTEM of tungsten carbide protected embedded in N-doped nanoporous carbon (denoted as WC@NPC) (inset: TEM image under lower magnification and particle-size distribution). (d) HER LSV curves in 0.5 mol L^{-1} H_2SO_4. (e) Free energy of H^* adsorption on different surfaces by DFT calculation. Adapted with permission from Ref. [78]. Copyright 2017, the American Chemical Society. (f) Procedure for the synthesis of the tungsten nitride (WN_x) NPs decorated on nitrogen-rich porous graphene-like carbon nanosheets (denoted as WN_x-NRPGC) composite. (g) TEM, and (h) HRTEM images of the WN_x-NRPGC composite. (i) LSV curves of the samples in 0.5 mol L^{-1} H_2SO_4 at a scan rate of 5 mV s^{-1}. Adapted with permission from Ref. [92]. Copyright 2018, Wiley-VCH Verlag GmbH & Co.

nocages and small apertures to confine the $W(CO)_6$ metal precursor. After pyrolysis at high temperature, tungsten carbide nanoclusters/NPs could be obtained, which have moderated H adsorption free energy and exhibit excellent HER performance in 0.5 mol L^{-1} H_2SO_4 (51 mV at 10 mA cm^{-2}, Tafel slope is 49 mV dec^{-1}) (Fig. 5d and e).

Similar to tungsten carbides, intensive attention was also attracted on molybdenum carbides. Kim *et al.* [79] synthesized Mo_2C, Fe_3C, and WC NPs loaded on rGO substrate for HER. Among these carbides, Mo_2C/rGO shows the best HER activity. Ma *et al.* [80] encapsulated uniform Mo_2C NPs (with size below 3 nm) with ultrathin graphene shells (1–3 layers). The cooperative/synergistic effects among Mo_2C, graphene shells, and the doped N contribute to the excellent HER performance in acidic media (a low onset potential (6 mV), a small Tafel slope (41 mV dec^{-1}), a large exchange current density (0.179 mA cm^{-2}) and a good stability (12 h)).

However, NPs are not an ideal form owing to the eventual activity loss when used in pristine form and the oxide-passivation in HER condition. Ko *et al.* [81] synthesized WC nanowalls for HER. No oxidation took place even after prolonged cycling tests (10,000 cycles) in the HER environment, suggesting the superior stability due to the highly crystalline and the smooth surface of the pristine WC nanowalls. Wu *et al.* [82] prepared mesoporous molybdenum carbide (MoC_x) nano-octahedrons composed of ultrafine nanocrystallites, which exhibit remarkable HER electrocatalytic performances in both acid and alkali. Humagain *et al.* [83] reported scalable synthesis of porous Mo_2C nanostructures. The Mo_2C catalyst exhibits an excellent HER activity (35 and 60 mV at 0 and 10 mA cm^{-2}, 60 mV at 100 mA cm^{-1}) and stability (>100 h at 10 and 100 mA cm^{-1}).

Transition metal nitrides

Transition metal nitrides have also attracted much attention as efficient HER electrocatalysts for their properties similar to noble metals. Many transition metal nitrides have been reported to show good HER properties, such as WN [84], Ni_3N [85,86], MoN [87], Co_xN [88], Fe_xN [89]. Yu *et al.* [90] synthesized various porous metallic nitrides on different substrates for HER in alkaline media. Compared with Fe_4N and Ni_3N, CoN is the best single-metal nitride for HER in 1 mol L^{-1} KOH (95 mV at 100 mA cm^{-2}, and 212 mV at 100 mA cm^{-2}). In addition, introducing Ni into CoN to form bi-metallic nitrides of NiCoN would further improve the HER activity (48 mV at 100 mA cm^{-2}, and 149 mV at 100 mA cm^{-2}). Titanium nitride (TiN), which shows good conductivity and corrosion resistance in aqueous solutions, is also considered as a promising catalyst for HER. Han *et al.* [91] directly synthesized single-crystalline TiN nanowires used a CVD method. The TiN nanowires are proved to be an efficient HER catalyst (92 mV at 1 mA cm^{-2}, Tafel slope, 54 mV dec^{-1}) with a good chemical stability (20,000 cycles and 100 h) in acid. Zhu *et al.* [92] coupled tungsten nitride (WN_x) with nitrogen-rich porous graphene-like carbon to optimize its HER activity. Benefiting from the nanostructured WN_x and the synergy, this catalyst exhibits a remarkable electrocatalytic performance (Fig. 5f–i).

Transition metal borides

Compared with the above-mentioned compounds, the reports with transition metal borides as active HER electrocatalyst do not attract so much attention. Actually, as early as 1992, Los and Lasia [93] used amorphous nickel boride for alkaline HER, but since then borides as active HER has not obtained considerable development which may be due to the difficult synthesis process [94]. Masa *et al.* [95] used amorphous cobalt boride (Co_2B) as an efficient alkaline HER electrocatalyst. Lu *et al.* [96] synthesized CoB NPs on CoO nanowire (CoB@CoO nanoarray), which displays high activity (102 mV to reach 50 mA cm^{-2}) and durability (the current density only degrades <17% after 20 h electrolysis) in 1.0 mol L^{-1} KOH. Zhang *et al.* [97] electrolessly plated NiB_x films for the HER in a wide pH range. The particle size and morphology of NiB_x are greatly affected by the atomic ratio of B to Ni, thus producing different electrocatalytic performances. $NiB_{0.54}$ (atomic ratio of Ni to B is 1:0.54) film is the optimal electrocatalyst with 45, 54 and 135 mV to reach the current density of 10 mA cm^{-2} in 0.5 mol L^{-1} H_2SO_4, 1.0 mol L^{-1} phosphate buffer solution (PBS, pH 7) and 1.0 mol L^{-1} KOH. Until 2012, molybdenum boride (MoB) was first reported as active HER catalysts by Vrubel *et al.* [98]. Park *et al.* [99] reported the synthesis and the HER electrocatalytic studies of Mo_2B, α-MoB, β-MoB, and MoB_2, and their results suggest the HER activity increases with the increase of boron content. Gupta *et al.* [100] synthesized Co-Ni-B nanocatalysts for electrocatalyzing HER in a wide pH range. The results suggest the molar ratio of Ni affects the activity greatly. Co-30Ni-B (with 30% Ni) has the best HER catalytic activity (170 mV at 10 mA cm^{-2}, pH 7, 133 mV at 10 mA cm^{-2}, pH 14). Xu *et al.* [101] deposited CoNiB NPs on Ni foam (CoNiB@NF), also showing good activity towards the HER.

STRUCTURE-ACTIVITY RELATIONSHIP OF NANOCATALYSTS IN ELECTROCHEMICAL HER

Modulation on microscopic structures (phase, size, and morphology)

The changes of chemical and structural parameters on microscopic structure (such as phase composition, size, shape/morphology) would also lead to changes in chemistry and structure on the surface, and would profoundly affect the catalytic performances, as the heterogeneous catalysis processes occurred on the surface [102]. Pan *et al.* [103] synthesized three crystalline phases of nickel phosphide ($Ni_{12}P_5$, Ni_2P, Ni_5P_4) (Fig. 6a–c), and found all of these catalysts are efficient for acidic HER, but the crystalline phase shows great effect on the HER electrocatalytic performance. The electrocatalytic activity follows the order of Ni_5P_4>Ni_2P>$Ni_{12}P_5$ (Fig. 6d), which can be ascribed to the different electronic properties of Ni and group effect of P—the highest positive charged Ni and the strongest group effect P in Ni_5P_4 led to the best HER performance. And their later research [104] suggests this crystalline phase effect also exists in cobalt phosphide materials. To give a clear comprehension on the effect of the crystalline phase on the HER performance, Callejas *et al.* [105] compared the HER performances of the different phase compositions of Co_2P and CoP NPs with the same morphology and size (thus minimizing contributions of morphologies to the HER) (Fig. 6e and f). Their results show that CoP gives a better HER catalytic activity than Co_2P because of the higher density of active sites introduced by the increased P contents in CoP (Fig. 6g). Even with the same atomic composition, the HER performance of transition metal chalcogenides is significantly affected by the phase. As widely recognized, 1T-phase MoS_2 or 1T-phase WS_2 shows superior HER catalytic performances than the corresponding 2H-phase by virtue of the enhanced charge transfer kinetics [50,106–108].

Nanocatalysts with different shapes have different crystallographic shapes, packing manners, densities and even electronic states, which essentially affect the catalytic performance [102]. On the other hand, HER involves processes among three phases (gas/water/solid). During the HER process, the formed H_2 bubbles may aggregate on the catalysts' surface, hindering the liquid mass transport and electron transfer, decreasing the number of exposed active sites, severely reducing the HER electrocatalytic performance. "Superaerophobicity" is an ideal surface state, which usually can be achieved by the formation of array architecture [109]. The study of Wang *et al.* [110] suggested that the morphology of the electrocatalyst surface greatly affect the equilibrium state of formation/detachment of the gas bubbles. Lu *et al.* [111] reported that MoS_2 nanostructures with vertically aligned MoS_2 nanoplatelets show a under-water "superaerophobic" surface, making the as-formed H_2 bubbles quickly driven off, and leading to a constant working area, thus greatly promoting the HER performance. Similarly, Li *et al.* [9] fabricated pine-shaped Pt nanostructures with under-water superaerophobicity, which showed a much higher HER performance than Pt nanospheres and flat electrodes.

Modulation on electronic structures

Introduction of foreign atoms into transition metal compounds can help modulate the electronic structures to improve the HER performances, and the introduced atoms can be cations or anions [112,113]. Wang *et al.* [114] investigated the HER performance of the cobalt-doped FeS_2 NSs/CNTs ($Fe_{0.9}Co_{0.1}S_2$/CNT), and they believed that doping metal atoms can effectively modify the electronic structure, thus optimizing the ΔG_{H^*} on the catalyst surface, accelerating the HER process. Hou *et al.* [115] constructed porous cobalt phosphorus selenide nanosheets (Fig. 6h–l) for HER, which showed good catalytic performances in alkaline media (150 and 180 mV at 10 and 20 mA cm^{-2}, respectively) (Fig. 6m). Theoretical calculations suggest that the replacement of Se around the vacancies by P atoms tunes the electronic structure of cobalt selenide, and optimizes the charge transfer and hydrogen desorption, thus promoting the kinetics (Fig. 6n).

Non-metal doping can also tune the electronic structures of electrocatalysts. Kibsgaard and Jaramillo [116] doped S into MoP, forming molybdenum phosphosulfide (MoP|S). The catalyst shows an improved HER activity over pure MoP; the team believed that S and P can optimize the electronic structure to enhance the electrocatalytic activity. Cabán-Acevedo *et al.* [117] suggested the doping of phosphorus on cobalt sulfides to form cobalt phosphosulfide (CoPS) can change the S_2^{2-} to $(SP)^{3-}$ dumbbells (Fig. 6o–r), which increases the surface electronic density, resulting in an optimized hydrogen adsorption, and thus enhancing HER process (Fig. 6s and t). Hong *et al.* [118] also synthesized a self-supporting nanoporous cobalt phosphosulfate (CoP|S) electrocatalyst for HER in alkaline and acidic media, and their theoretical studies confirm the substitution of P by S can modify the electronic structures of the catalyst, thereby improv-

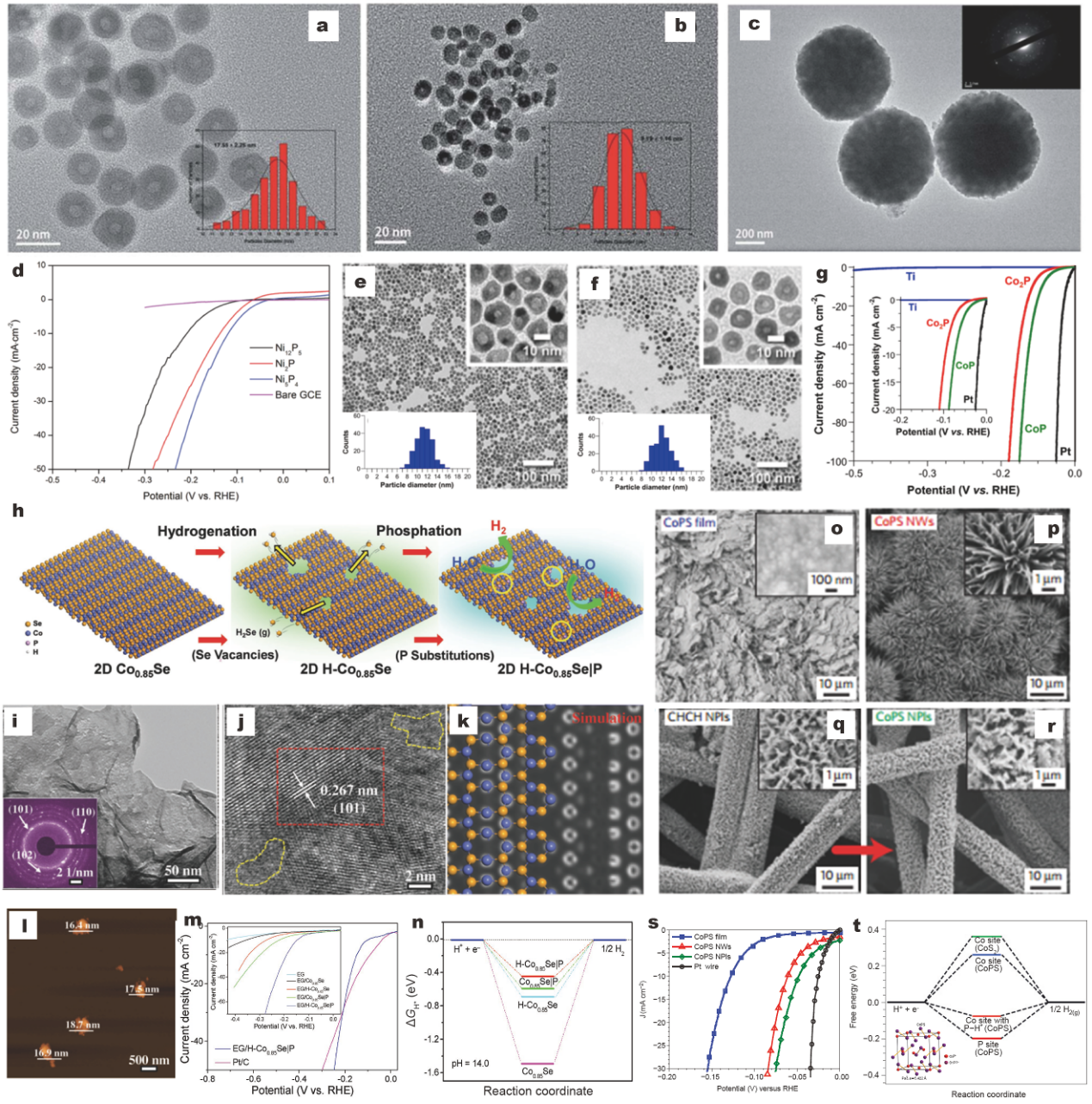

Figure 6 TEM images of nickel phosphide nanocrystals with different phases: (a) $Ni_{12}P_5$, (b) Ni_2P, and (c) Ni_5P_4. The size distributions of $Ni_{12}P_5$ and Ni_2P are shown in the insets in (a) and (b). The selected area electron diffraction (SAED) pattern of Ni_5P_4 is shown in the inset in (c). (d) LSV curves of the samples in 0.5 mol L^{-1} H_2SO_4. Reproduced with permission from Ref. [103]. Copyright 2015, the Royal Society of Chemistry. TEM images of (e) Co_2P and (f) CoP, with enlarged regions and size distribution in the insets. (g) LSV curves in 0.5 mol L^{-1} H_2SO_4 for Co_2P/Ti and CoP/Ti electrodes, along with Pt mesh and bare Ti foil for comparison. Adapted with permission from Ref. [105]. Copyright 2015, the American Chemical Society. (h) Schematic illustration for the synthesis process of H-$Co_{0.85}$Se|P. (i) TEM and (j) HRTEM images of H-$Co_{0.85}$Se|P. Inset in (i): SAED pattern of H-$Co_{0.85}$Se|P. (k) Simulated scanning TEM image of the $Co_{0.85}$Se. (l) Atomic force microscopy (AFM) image of H-$Co_{0.85}$Se|P on silicon substrate. (m) LSV curves of the samples for HER. (n) DFT-calculated free-energy diagrams of the HER. Adapted with permission from Ref. [115]. Copyright 2017, Wiley-VCH Verlag GmbH & Co. SEM images of as-synthesized CoPs film (o) and CoPS NWs (p) on graphite, and cobalt hydroxide carbonate hydrate nanoplates (CHCH NPIs) on carbon fiber paper before (q) and after (r) thermal conversion into CoPS NPIs. (s) LSV curves of the samples. (t) Free-energy diagram. Reproduced with permission from Ref. [117]. Copyright 2015, Nature Publishing Group.

ing the HER activity.

Modulation on d-band centers

HER falls in the category of heterogeneous catalysis, which occurs on the surface of the catalyst through the key hydrogen adsorption step, and an ideal hydrogen adsorption commonly indicates a good electrocatalytic HER activity. DFT calculations suggest the d-band center could largely describe the adsorbate-metal interaction on catalyst surfaces. The coupling between the valence state of the adsorbate and the d-band of the transition metals greatly reflects the adsorption energy variation of the adsorbate. The higher-energy d states relative to the Fermi energy (the highest occupied state) of the transition metals indicate the stronger interaction with the adsorbate [102], and vice versa. Chen *et al.* [119] used transition metal V doping to tailor the d-band center of Co_4N NSs (Fig. 7a), thereby facilitating the H desorption, and leading to an enhanced HER electrocatalytic activity (37 mV at 10 mA cm^{-1}) (Fig. 7c), even comparable to Pt/C catalysts. Through a series of characterizations, especially Co L-edge X-ray absorption near edge structure (XANES) (Fig. 7b), ultraviolet photoelectron spectroscopy (UPS), and DFT calculations, they suggested that the improved HER electrocatalytic activity is because of the downshift of the d-band center, which weakens the adsorption of hydrogen. The DFT calculations suggest V doped Co_4N shows d-band center which is much farther away from the Fermi level than Co_4N (the d-band centers for Co_4N and V doped Co_4N relative to the Fermi energy are −1.79 and −1.85 eV, respectively) (Fig. 7d), and more electrons fill the anti-bonding states after V doping, facilitating the hydrogen desorption, thereby optimizing the ΔG_{H^*} (Fig. 7e). Pan *et al.* [120] used a self-template conversion method to synthesize a CoP hollow polyhedron frame (HPF) catalyst doped with foreign metal (Fig. 7f). It is found that the doping of Ni can effectively optimize the electronic structure and d-band center of CoP, and the L-edge absorption of Co shifts negatively after metal doping (Fig. 7g), indicating that the electron transfer from the doped metal to the Co atom makes the electron density around the Co atom higher, which is conducive to the HER progress (Fig. 7h). The ΔG_{H^*} after Ni doping is close to 0 eV, indicating that it has more suitable hydrogen binding energy (Fig. 7i). Besides, the doping of Ni makes the d-band center downshift from Fermi level (Fig. 7j), thus reducing the hydrogen adsorption energy, promoting the desorption of H from the catalysts' surface and improving the HER performance.

Design and engineering on heterointerfaces

Recently, many researchers are focusing on constructing heterostructures for HER. Rational design and controllable synthesis of heterostructured catalysts with the ideal heterointerfaces can selectively integrate the advantages of different components, overcome the shortcomings of the single components, so as to achieve superior electrocatalytic performances, and the formed heterointerfaces even may give unexpected performances and effects [121]. Most of the reported heterostructured catalysts can be divided into two classes, active/active and active/non-active, both showing enhanced electrocatalytic performances than their counterparts for the following superiorities [122].

(1) Most of the reported heterostructures show well-defined nanostructures, substantially exposing active sites, which can offer more adsorption sites for hydrogen intermediates. Lin *et al.* [123] recently reported CoP/NiCoP nanotadpoles (NTs)-like heterojunction (Fig. 7k and l) for efficient electrocatalytic HER over a wide pH range (Fig. 7m and n). Characterizations suggested the CoP/NiCoP NTs possess rich heterointerfaces between CoP and NiCoP, which may expose more active sites for HER. DFT calculations proved that an optimized ΔG_{H^*} and H_2O dissociation are achieved at the heterointerface, accelerating the HER reaction in electrolytes with different pH values.

(2) Introducing bulk (such as carbon cloth/paper, nickel foam, Ti foils) or nanosized (such as CNTs, graphene-based materials or graphitic carbon nitride, 2D transition metal dichalcogenide) substrates to form active/non-active heterostructures is a widely used and readily implementable strategy to construct efficient HER electrocatalysts, which can not only enhance the conductivity and accelerate the mass diffusion in the electrocatalytic process, but also offer a higher specific surface area to disperse the active species, exposing more active sites, meanwhile, avoiding the agglomeration, thus improving both the activity and stability.

(3) The stability of the catalysts can also be improved by the construction of heterostructures. For example, through the formation of the well-defined core@shell structures, the stable species can protect the other active but not stable species. Lin *et al.* [124] synthesized multi-dimensional Ni/NiCoP nano-heterojunctions (NHs). In this heterojunction structure, Ni NPs are enclosed and then strung by single-phased NiCoP, forming strings of snap bean-like core@shell structures. This particular structure not only takes the most of advantages of Ni metal and bimetallic phosphides nanostructures, but also

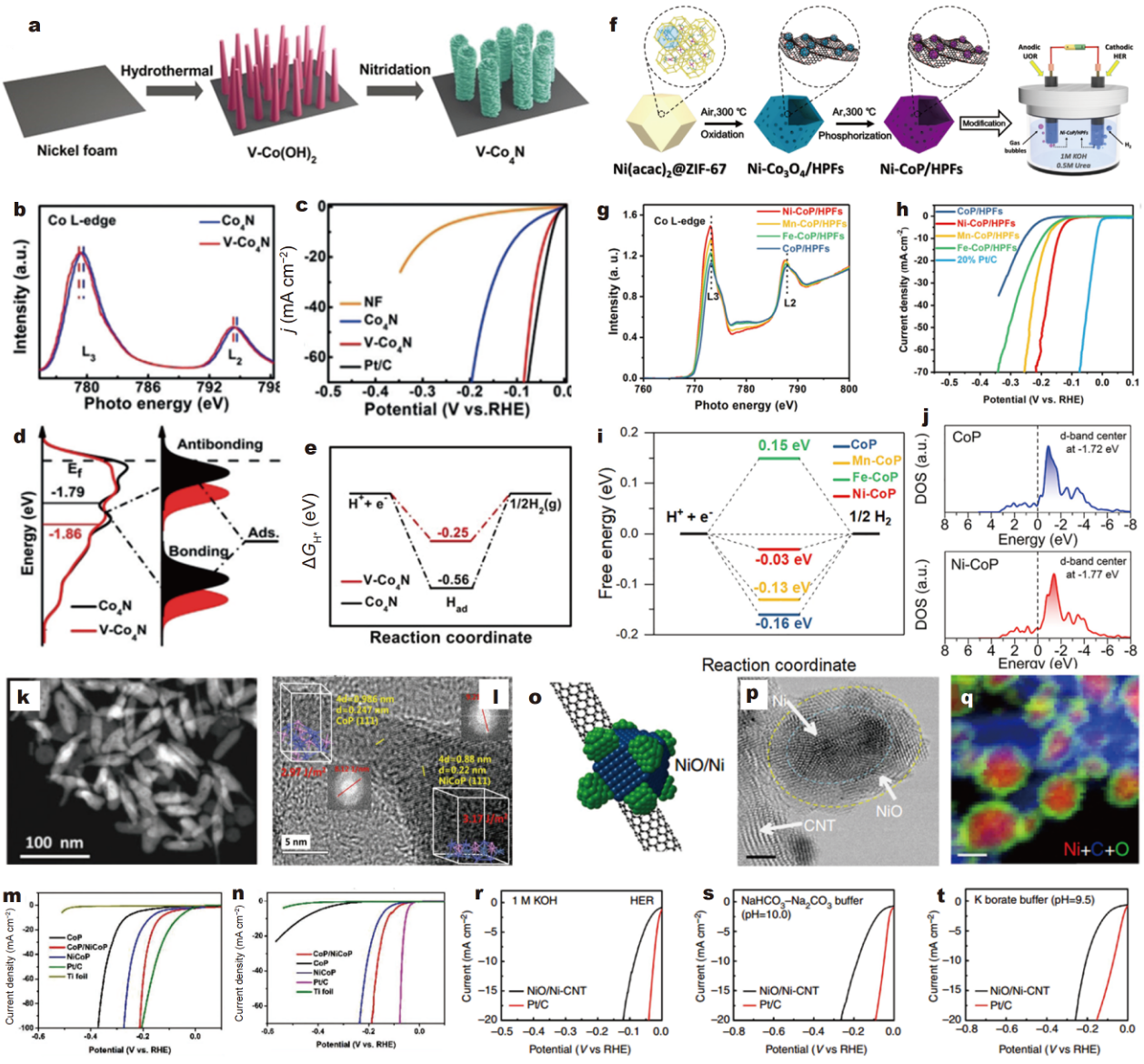

Figure 7 (a) Schematic representation of the preparation of a V-Co_4N NS. (b) XANES Co L-edge spectra for Co_4N and V-Co_4N. The dashed lines highlight the peak positions. (c) LSV of Ni foam, Co_4N, V-Co_4N, and Pt/C. (d) The DOS plots of Co_4N and V-Co_4N as well as the corresponding schematic illustration of bond formation between the reaction surface and the adsorbate. The d-band centers are also highlighted in the DOS curves. (e) Free-energy diagram for the HER on Co_4N and V-Co_4N. Adapted with permission from Ref. [119]. Copyright 2018, Wiley-VCH Verlag GmbH & Co. (f) Schematic illustration of the Ni-CoP/HPFs. (g) XANES spectra at the Co L-edge of CoP/HPFs and M-CoP/HPFs. (h) LSV curves in 0.5 mol L^{-1} H_2SO_4. (i) The calculated free-energy diagram of Ni-CoP, Mn-CoP, Fe-CoP and CoP. (j) Calculated DOS curves for CoP and Ni-CoP. Reprinted with permission from Ref. [120]. Copyright 2019, Elsevier. (k) HAADF-STEM and (l) HRTEM (inset shows the calculated surface energies and FFT images of CoP and NiCoP) of CoP/NiCoP NTs. LSV curves in (m) 1 mol L^{-1} KOH and (n) 0.5 mol L^{-1} H_2SO_4. Adapted with permission from Ref. [123]. Copyright 2019, Wiley-VCH Verlag GmbH & Co. (o) A schematic illustration of the NiO/Ni-CNT structure. (p) Atomic resolution STEM bright-field image showing the structure of a typical NiO/Ni particle on a CNT (small NiO NPs over a larger Ni nanoparticle core). Scale bar, 2 nm. (q) Reconstructed elemental maps with Ni in red, C in blue and O in green for (d) NiO/Ni-CNT, scale bar is 5 nm. (r) LSV curves of NiO/Ni-CNT and Pt/C in (s) 1 mol L^{-1} KOH, (t) $NaHCO_3$-Na_2CO_3 buffer (pH 10.0) and (j) potassium borate buffer (pH 9.5). Reproduced with permission from Ref. [24]. Copyright 2014, Nature Publishing Group.

avoids the disadvantages (Ni is high conductivity, but easy to corrode and unstable in electrolyte; bimetallic phosphides have high activity and stability, but with poor conductivity). Thus, the activity and stability are both

elevated.

(4) The different components in heterostructures show different electronegativities, and lead to the electronic redistribution between different components, which can tune the electronic structure or the band structures of the electrocatalysts, thereby enhancing the catalytic performance for HER. The electronic redistribution can be well reflected by the XPS, especially the synchrotron-radiation-based X-ray absorption spectroscopy (XAS). Recent studies suggested that the formation of the hetero-interfaces in heterostructured Ni/NiCoP NHs and CoP/NiCoP NTs can tune the electronic structures of the catalysts, thus promoting the HER process [123,124].

Besides, synergistic effect between different components (which may be reflected indirectly in the above four factors) is also an important factor that, as most of relevant researchers have stated, contributes greatly to the enhancement of HER electrocatalytic performance. Gong *et al.* [24] constructed nickel oxide/nickel heterostructures on carbon nanotube sidewalls (Fig. 7o–q), which showed a high HER electrocatalytic performance (Fig. 7r–t) even similar to that of Pt/C in 1 mol L^{-1} KOH. Based on DFT calculation results, they believed that the formation and desorption of OH^- may be a key step in alkaline HER process. On the hetero-interface of the nickel oxide/nickel heterostructures, synergy between Ni and NiO is responsible for the excellent HER activity. By virtue of the stronger electrostatic affinity and more unfilled d orbitals in Ni^{2+} of NiO than in Ni metal, OH^- is more inclined to adsorb on the NiO sites, whereas the nearby Ni sites benefit the H adsorption. The synergy between the two components promotes the alkaline HER process. Wang *et al.* [125] reported 1D metal/sulfide heterostructures (PtNi/NiS) for acidic and alkaline HER. DFT was used to calculate the energy barrier for H_2O dissociation (breaking the OH–H bond), and the result suggests Pt (111) surface has a much higher energy barrier (0.89 eV) than NiS (100) surface (0.32 eV), indicating that the NiS surface can promote the step of water dissociation, and then promote the formation of the H_{ads}. Pt_3Ni (111) shows a ΔG_{H^*} value (0.09 or 0.13 eV) closer to 0 than that of NiS (100) (0.56 eV), suggesting that Pt_3Ni is beneficial for producing H_2. In brief, the synergy between Pt_3Ni and NiS contributes greatly to the enhanced HER activity in alkaline. NiS shows a stronger electrostatic affinity to adsorb the OH^- and avoid blockade of the active sites on Pt by virtue of the unfilled d orbitals on Ni^{2+}, and the produced H^+ adsorbed on the nearby spare Pt sites for the subsequent H_2 formation.

SINGLE-ATOM SITE CATALYSTS ENGINEERING FOR HER

Noble-metal-based SASCs

Pt SASCs

Metallic Pt is thus far recognized as the most active HER catalyst. In this regard, currently the main tasks are to further elevate its activity and reduce its loading in the overall catalyst. The emerging concept of "single-atom catalysis" offers a feasible solution to the above issues. Single-atom catalysts (SACs) can be considered as supported catalysts with their catalytic entities downsized to the extreme, and thus can maximize the utilization efficiency of noble metals. Therefore, single-atom Pt are the most frequently reported HER catalysts featuring single atoms of noble metals. Liu *et al.* [126] designed a SAC with Pt atoms anchored on onion-like carbon spheres (denoted as Pt_1/OLC) (Fig. 8a–d), with a Pt loading as low as 0.27 wt%. In 0.5 mol L^{-1} H_2SO_4, the Pt_1/OLC catalyst gives a low overpotential (38 mV at 10 mA cm^{-2}) and a high TOF value (40.78 H_2 s^{-1} at 100 mV) (Fig. 8e and f). These data are not only superior to those for the Pt_1/graphene catalyst with a similar Pt loading (0.33 wt%) obtained *via* the same preparation method, but also comparable to those for commercial Pt/C catalyst with a loading of 20 wt%. XANES and EXAFS combined with HRTEM have revealed that, benefiting from the high surface curvature of the OLC support, the single-atom Pt sites have a local electric field effect. This unique structure attracts protons to concentrate at the Pt sites, and promotes the proton coupled electron transfer process, leading to outstanding HER performances. This work presents a new strategy to elevate the activity of single-atom sites by modulating the nanostructure of carbon support. Zhang *et al.* [127] reported an *in situ* electrochemical exfoliation method (Fig. 8g) to anchor single Pt atoms on $Mo_2TC_2T_x$ support during the HER process. In the obtained catalyst, each Pt atom occupies a Mo vacancy in the support, and forms three Pt–C bonds with adjacent C atoms (Fig. 8h and i). In 0.5 mol L^{-1} H_2SO_4, the catalyst gives an overpotential as low as 30 mV at 10 mA cm^{-2}. The mass activity is 40 times as high as that for commercial 20% Pt/C catalyst (Fig. 8j and k). Also, the catalyst displays an outstanding stability during the electrocatalytic test, with barely any decline in activity after 10,000 cyclic voltammetry cycles or 100 h chronoamperometry. Ye *et al.* [128] developed a simple microwave-assisted method to reduce Pt precursor into single atoms supported on aniline-stacked graphene (Pt

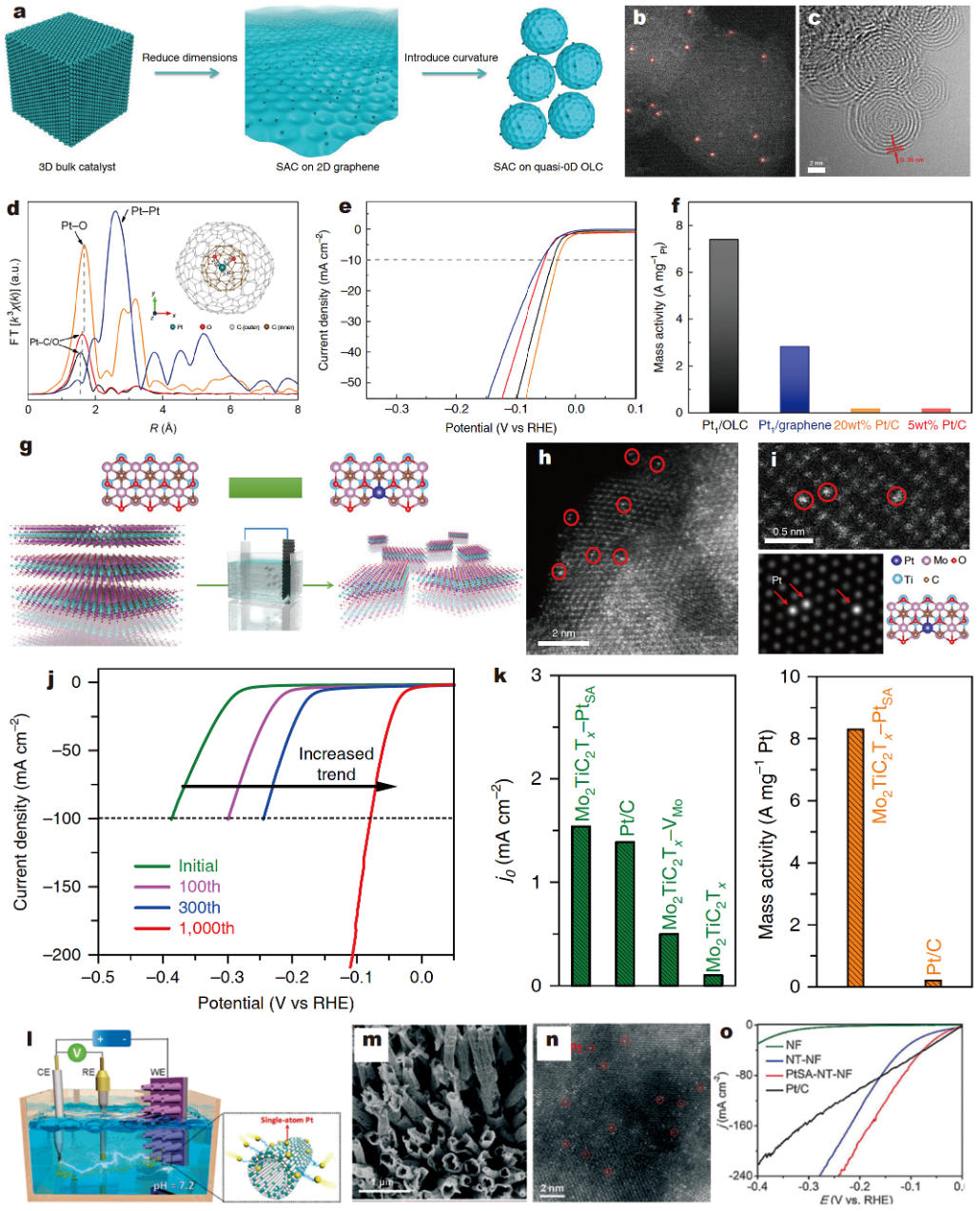

Figure 8 (a) The schematic illustration of Pt_1/OLC. (b) Spherical aberration (AC) corrected HAADF-STEM and (c) HRTEM images of Pt_1/OLC. (d) The Pt L_3 edge FT-EXAFS spectra of Pt_1/OLC (red), along with PtO_2 (yellow), Pt foil (blue) and the Pt ligands/OLC (black) (without O_3 exposure to remove their ligands in $MeCpPtMe_3$ precursors) for comparison. Inset: the optimized atomic model of PtO_2C_{295}, which exhibits Pt–O bonding in accordance with the experiments, where the grey and brown balls represent the carbon atoms in the outer/inner shell of fullerene-like structure. (e) LSV curves of Pt_1/OLC (black) in comparison with 5 wt% and 20 wt% commercial Pt/C (red and orange, respectively) and Pt_1/graphene (0.33%) (blue) in a 0.5 mol L^{-1} H_2SO_4 electrolyte. (f) The mass activity of Pt_1/OLC is normalized to the Pt loading at an overpotential of 38 mV with respect to the reference catalysts. Reproduced with permission from Ref. [126]. Copyright 2019, Nature Publishing Group. (g) Schematic of the electrochemical exfoliation process of MXene with immobilized single Pt atoms. (h) AC-HAADF-STEM image of $Mo_2TiC_2T_x$-Pt_{SA}. (i) Magnified HAADF-STEM image of $Mo_2TiC_2T_x$-Pt_{SA} and its corresponding simulated image, and illustration of the structure of $Mo_2TiC_2T_x$-Pt_{SA}, showing the isolated Pt atoms (circles in (g) and (h)). (j) HER LSV curves of the samples in 0.5 mol L^{-1} H_2SO_4 solution. (k) Exchange current densities of the catalysts, and the mass activities of state-of-the-art Pt/C and $Mo_2TiC_2T_x$-PtSA. Reproduced with permission from Ref. [127]. Copyright 2018, Nature Publishing Group. (l) Schematic diagram of the synthesis process. CE: counter electrode; RE: reference electrode; WE: working electrode. The CE is Pt. (m) SEM image of a piece of Pt_{SA}-NT-NF. (n) AC-HAADF-STEM of Pt_{SA}-NT-NF. (o) HER polarization curves of NF, NT-NF, Pt_{SA}-NT-NF, and Pt/C in N_2-saturated 1.0 mol L^{-1} PBS. Adapted with permission from Ref. [130]. Copyright 2017, Wiley-VCH Verlag GmbH & Co.

SASs/AG, with a Pt loading of merely 0.44%). The catalyst gives an excellent HER activity (an overpotential of 12 mV at 10 mA cm^{-2}; at an overpotential of 50 mV, the mass activity reaches up to 22,400 A $g(Pt)^{-1}$, 46 times as high as that for commercial 20 wt% Pt/C). Zhang *et al.* [129] reported a novel dynamic reaction approach to relocate the single Pt atoms on the surface of the precursor (carbon spheres) into the interiors of the porous carbon matrix (PCM). HER tests reveal that the Pt atoms immobilized in the crystal lattice of PCM display outstanding performances in both acid and alkali.

Pt-based SACs can also give high HER performance under neutral conditions. Zhang *et al.* [130] found that during the electrocatalytic reaction (Fig. 8l), the Pt atoms on Pt anode can be dissolved into the electrolyte and then deposited on the cathode; by exploiting this process, they developed a novel potential-cycling method, and prepared Pt atoms on CoP-based nanotube (NT) arrays supported by a Ni foam (NF) (denoted as PtSA-NT-NF) (Fig. 8m–n). For HER in neutral electrolyte (pH 7.2), the catalyst gives an overpotential of 24 mV at 10 mA cm^{-2} (Fig. 8o); at an overpotential of 50 mV, the mass activity reaches 70 A g^{-1}, which is four times of that for commercial 20 wt% Pt/C. Also, the catalyst displays a low Tafel slope (30 mV dec^{-1}) and a high stability. This method is also proved to be a general preparation method for Pt-based SACs, with a range of materials applicable as the cathode. Jiang *et al.* [131] employed a similar route and prepared a catalyst comprising single Pt atoms supported on nanosized porous cobalt selenide (Pt/np-$Co_{0.85}Se$). In neutral electrolyte (pH 7), the catalyst also displays an HER electrocatalytic performance superior to those of commercial Pt/C. By operando XAS and DFT calculations, the team identified that the high HER activity originates from the synergy between single Pt atoms and np-$Co_{0.85}Se$.

Ru SASCs

Besides Pt, single atoms of other noble metals (such as Ru) have also been reported as catalysts for HER. Yang *et al.* [132] employed phosphorus nitride (PN) nanotubes as support, and thereupon anchored single Ru atoms *via* the interaction between the d orbitals of Ru and the lone-pair electrons of N. The resulting catalyst displays a high HER activity in acid, with an overpotential of 24 mV at 10 mA cm^{-2}, a Tafel slope of 38 mV dec^{-1}. The TOF reaches 1.67 and 4.29 H_2 s^{-1} at 25 and 50 mV, respectively. The catalyst also exhibits a good stability at a current density as large as 160 mA cm^{-2}. Ramalingam *et al.* [133] used 2D titanium carbide ($Ti_3C_2T_x$) MXene as an effective carrier to load Ru single atoms (RuSA-N-S-$Ti_3C_2T_x$) (Fig. 9a–d). Through the formation of the Ru–N, Ru–S bonds to stabilize Ru single atom (Fig. 9e). And the synthesized RuSA-N-S-$Ti_3C_2T_x$ shows outstanding HER electrocatalytic performance in acid, which only needs 76 mV to reach 10 mA cm^{-2} (Fig. 9f). Theoretical calculation suggests the activity enhancement derives from the coordination effect of N and S in Ru and $Ti_3C_2T_x$ MXene (Fig. 9g and h). Therefore, Ru-based SACs for HER can also display superior activity and stability to those of commercial Pt/C. Considering that Ru is far less expensive than Pt, these Ru-based SACs are expected to play a major role in future large-scale HER-related applications. Besides the SACs based on noble metals, Zhang *et al.* [134] also prepared bimetallic dimer structures (Pt-Ru dimers) for acidic HER, showing higher HER activity (>50 times higher than that of the commercial Pt/C) and excellent stability due to the synergy effect.

Ir SASCs

Lai *et al.* [135] used the π electrons on imidazole group of ZIF-67 to bond metal ions M (M=Ir, Pt, Ru, Pd, Fe, Ni) to form single-atom sites on a heterogeneous support composed by the nitrogen-doped carbon matrix (N/C) and Co NPs. The single-atoms can simultaneously anchor on these two distinct domains, forming M@NC, and centers of M@Co. The single-atom Ir catalyst exhibits the best electrocatalytic performance. DFT calculations indicate that the Ir@Co sites benefit the OER, while the Ir@NC_3 sites promote the HER process, accelerating the full water splitting.

None-noble-metal-based SASCs

Ni SASCs

Zhang *et al.* [136] reported a catalyst featuring single Ni atoms anchored on defective graphene (A-Ni@DG), which displays a high activity for electrochemical water splitting. For OER in acid (0.5 mol L^{-1} H_2SO_4) and alkali (1 mol L^{-1} KOH), the catalyst displays an overpotential of 70 and 270 mV at 10 mA cm^{-2}, respectively, far superior to commercial Ir/C catalyst, and the HER activity is close to that of commercial Pt/C as well. Li *et al.* [137] reported a single-atom tailoring strategy to prepare Pt nanowires decorated with single Ni atoms (denoted as SANi-PtNWs) (Fig. 9i–l). Most activated Pt sites were created with adjacent nickel atoms, which endow the catalyst with a high HER activity in alkaline media. At an overpotential of −70 mV, the mass activity reaches 11.8±0.43 A $mg(Pt)^{-1}$, far surpassing the

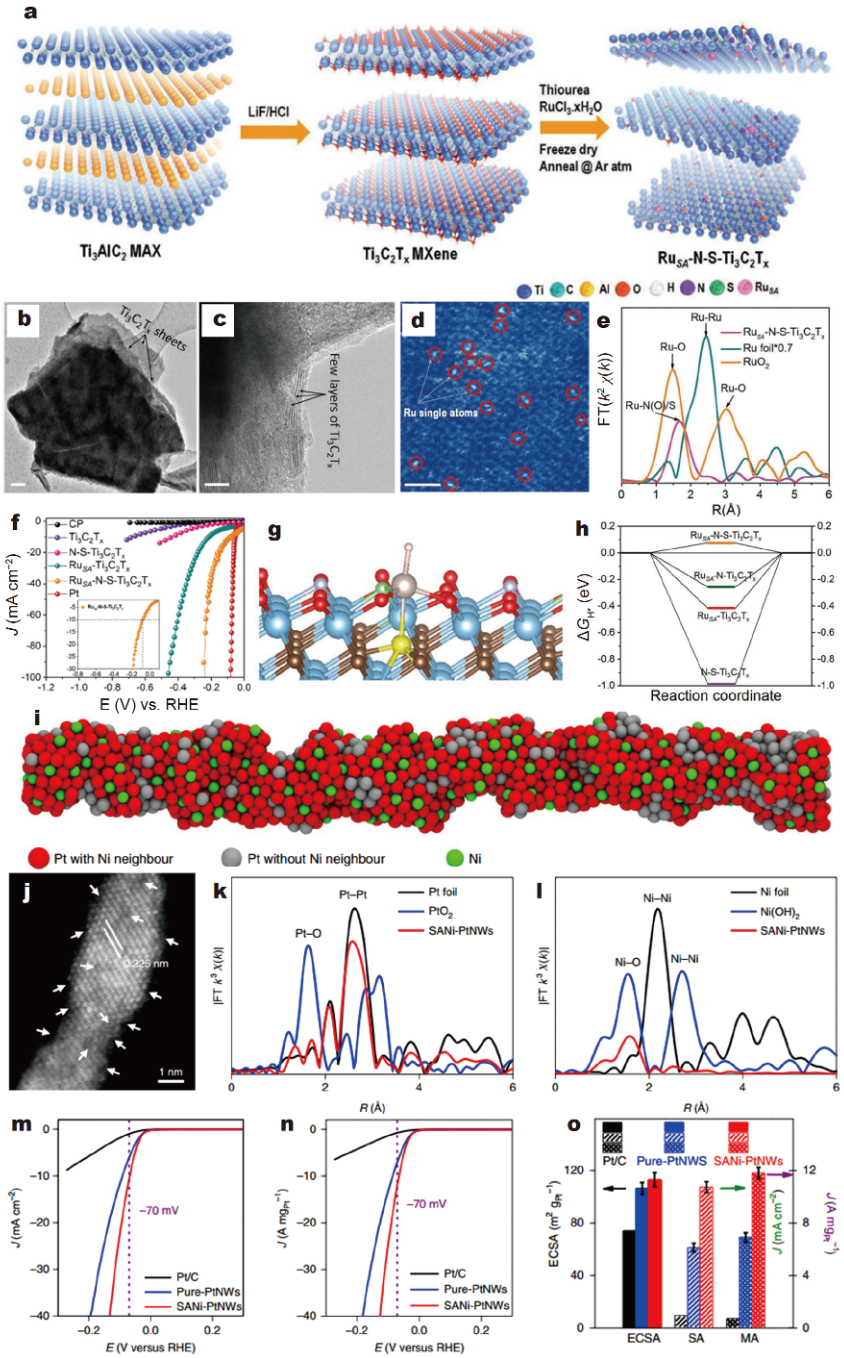

Figure 9 (a) Schematic illustration of the synthesis route of RuSA-N-S-$Ti_3C_2T_x$ catalyst. (b) TEM image of RuSA-N-S-$Ti_3C_2T_x$ shows the 2D $Ti_3C_2T_x$ NSs. Scale bar, 200 nm. (c) HRTEM image of few-layered RuSA-N-S-$Ti_3C_2T_x$, scale bar, 20 nm. (d) AC-HAADF-STEM image of RuSA-N-S-$Ti_3C_2T_x$ (bright dots marked with red circles indicate the Ru_{SA} on the $Ti_3C_2T_x$ MXene support). Scale bar, 2 nm. (e) The FT-EXAFS spectra. (f) HER LSV curves of the catalysts in 0.5 mol L^{-1} H_2SO_4. Inset: the magnified view of the HER polarization curve of Ru_{SA}-N-S-$Ti_3C_2T_x$. (g) Atomic model of the Ru_{SA}-N-S-$Ti_3C_2T_x$ catalyst (blue, brown, red, light blue, yellow, green, and gray colored balls represent Ti, C, O, F, S, N, and Ru atoms, respectively). (h) The calculated ΔG_{H^*} diagram. Adapted with permission from Ref. [133]. Copyright 2019, Wiley-VCH Verlag GmbH & Co. (i) Schematic diagram and (j) HAADF-STEM image of SANi-PtNWs. White arrows highlight the surface defects, steps and concave cavity sites. (k) Pt EXAFS fitting result. (l) Ni EXAFS fitting result. ECSA normalized (m) and Pt mass loading normalized (n) HER LSV curves. (o) Comparison of ECSA (black arrow, left axis), SA values (normalized by ECSA, green arrow, right axis) and MAs (normalized by Pt mass, purple arrow, right axis) for HER at −70 mV *versus* RHE for all tested materials. Reproduced with permission from Ref. [137]. Copyright 2019, Nature Publishing Group.

team's previous record (3.03 A mg(Pt)$^{-1}$ for excavated PtNi nanomultipods) and the then-world-record (7.23 A mg(Pt)$^{-1}$ for PtNi-O octahedra) (Fig. 9m–o). Lou's group [138] reported the partial replacement of Mo atoms in MoS_2 by single Ni atoms *via* surface modification, which could effectively optimize the electronic structures of activated S atoms in the basal plane, unleashing their inherent activity. To sum up, the introduction of single Ni atoms is a general and effective approach to preparing high-performance HER catalysts. Besides, on the basis of first principle calculations, Ling *et al.* [139] designed the first "single-atom bifunctional" catalyst for electrochemical water splitting. The catalyst features single Ni atoms anchored in β_{12} boron monolayer with unique geometry, and is expected to show competence for overall water splitting.

Fe SASCs

Xue *et al.* [140] employed graphdiyne as support, and thereupon loaded Fe(0) and Ni(0) atoms with atomic dispersion, by taking advantage of the C≡C bonds, large surface area and high porosity of graphdiyne (GD) (Fig. 10a–d). The resulting Fe(0)/GD and Ni(0)/GD catalysts show high activity and stability in HER test, with overpotentials of 66 and 88 mV at 10 mA cm^{-2} (Fig. 10e), respectively. At an overpotential of 0.2 V, the mass activities of these two catalysts are 34.6 and 7.19 times as high as that for commercial 20% Pt/C (Fig. 10f), with the upper limit number of the active sites of 2.56×10^{16} sites per cm^2 and 2.38×10^{16} sites per cm^2, 17 and 15.8 times as high as that for Pt(111) (1.5×10^{15} sites per cm^2). This work offers a new strategy for the development and application of zero-valence single-atom metals. Pan *et al.* [141] reported a polymerization-pyrolysis-evaporation approach and prepared a catalyst with single Fe atoms anchored on N-doped porous carbon. AC-HAADF-STEM, EXAFS and ^{57}Fe Mossbauer spectroscopy confirmed the active sites with a Fe-N_4 structure. The catalyst displays a good HER electrocatalytic performance in alkaline electrolyte (1 mol L^{-1} KOH).

Co SASCs

Fei *et al.* [142] published the first report of anchoring single Co atoms on N-doped graphene. By AC-HAADF-STEM and EXAFS, they revealed that the bonding between Co and N can promote the HER process. This catalyst displays high activity and stability in both acid (0.5 mol L^{-1} H_2SO_4) and alkali (1 mol L^{-1} KOH), with an overpotential of 147 and 270 mV at 10 mA cm^{-2}, respectively. This team [143] also reported the fast, microwave-assisted preparation (within 2 s) of N-doped graphene supporting different single metal atoms (Co, Ni, Cu). Compared with those obtained *via* conventional thermolysis, the catalysts obtained with this microwave-assisted method feature less ordered coordination environments around the single metal atoms, and a higher degree of defects. The corresponding Co-based catalyst displays an exceptional HER catalytic performance, with an onset potential close to 0, a Tafel slope of 80 mV dec^{-1}. At a current density of 10 mA cm^{-2}, the overpotential is only 175 mV. Sun *et al.* [144] employed a dual-template cooperative pyrolysis approach (Fig. 10g) and prepared a catalyst comprising highly dispersed Co single-atom-site (SAS) embedded on hierarchically ordered porous N-doped carbon (HOPNC) (denoted as Co-SAS/HOPNC) (Fig. 10h–l). The Co-N_4 active sites can effectively alter the electronic structure of the catalyst, and confer a high HER performance in acidic media (Fig. 10m), with an overpotential of 137 mV at 10 mA cm^{-2}. At overpotentials of 100 and 200 mV, the TOF reaches 0.41 and 3.8 s^{-1}, respectively. The catalyst also displays a good stability.

Mo SASCs

Chen *et al.* [145] reported a catalyst with single Mo atoms loaded on N-doped carbon, with $Mo_1N_1C_2$ active sites. For HER in alkaline electrolyte (0.1 mol L^{-1} KOH), this catalyst displays a higher activity than Mo_2C and MoN, with an onset potential of merely 13 mV. At a current density of 10 mA cm^{-2}, the overpotential is only 132 mV. Also, the catalyst has a higher stability than Pt/C. Compared with Mo_2C, MoN and N-doped graphene, the $Mo_1N_1C_2$ catalytic site also showed the lowest absolute value of ΔG_{H^*}, as demonstrated by DFT results.

W SASCs

Chen *et al.* [146] designed and prepared a metal-organic frameworks (MOF)-derived catalyst with N-doped carbon supporting single W atoms (denoted as W-SAC). AC-HAADF-STEM and EXAFS confirmed that the active sites exist in the form of $W_1N_1C_3$. The catalyst gives a high activity and stability for HER in both acidic and alkaline conditions. In 0.1 mol L^{-1} KOH, the overpotential is 85 mV at 10 mA cm^{-2}, only 5 mV higher than that for commercial Pt/C; the Tafel slope is 53 mV dec^{-1}. In 0.5 mol L^{-1} H_2SO_4, the overpotential is 105 mV at 10 mA cm^{-2}, and the Tafel slope is 58 mV dec^{-1}. DFT calculation suggested the $W_1N_1C_3$ moiety played an important role in optimizing hydrogen adsorption free energy, thereby enhancing the HER performance.

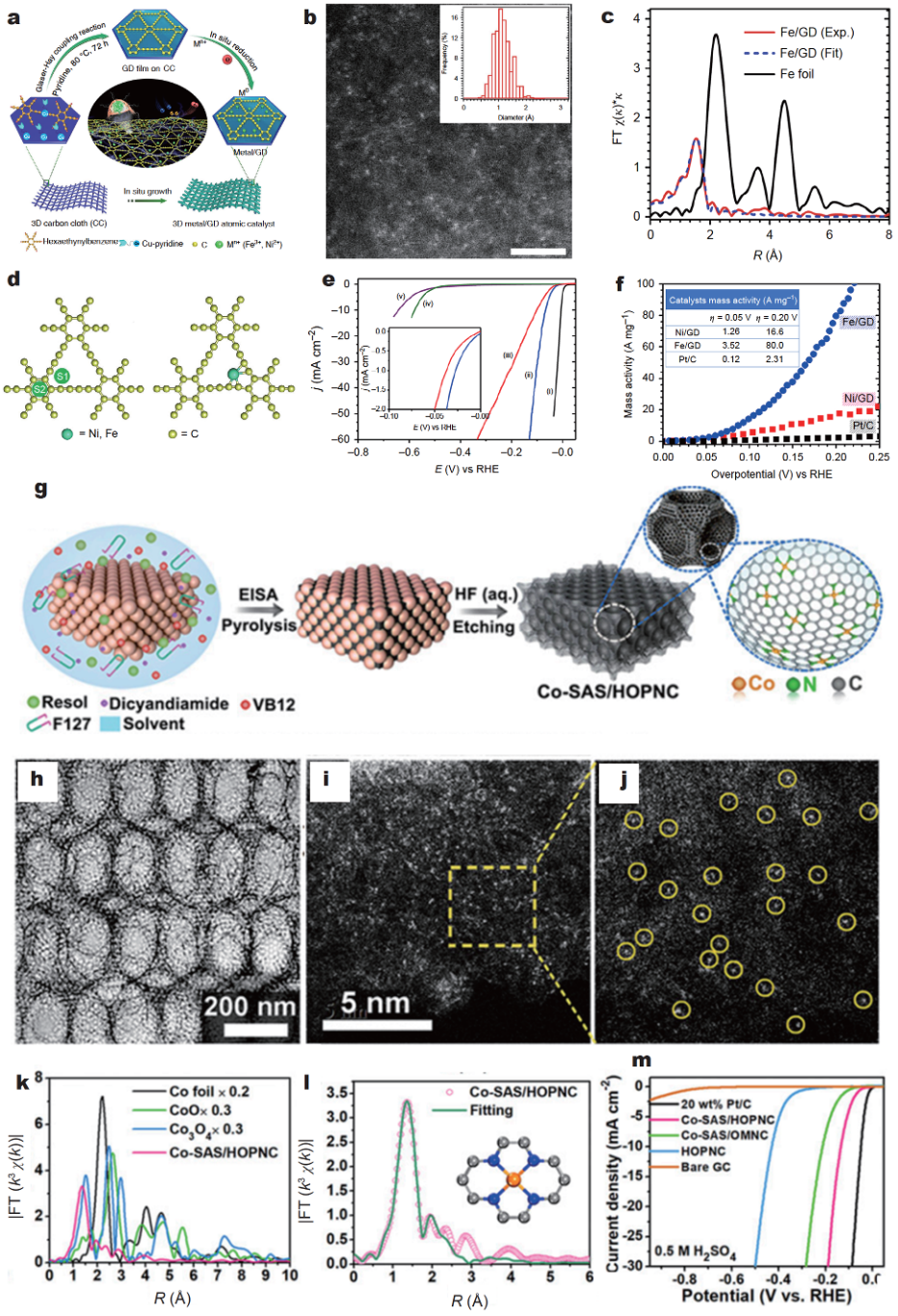

Figure 10 (a) Synthesis protocols for Ni/GD and Fe/GD. (b) AC-HAADF-STEM image of Fe/GD (inset: size distribution of Fe atoms counted from AC-HAADF-STEM images, (>1070 Fe atoms considered, the most probable value is 1.02 ± 0.33 Å)). Scale bar, 2 nm. (c) *Ex situ* EXAFS spectra of Fe/GD and Fe foil at the Fe K-edge. (d) Adsorption of single metal atoms on GD (left: possible adsorption sites; right: optimized configuration). (e) LSV curves of (i) Pt/C, (ii) Fe/GD, (iii) Ni/GD, (iv) GDF, and (v) CC (inset: enlarged view of the LSV curves for Fe/GD and Ni/GD near the onset region). (f) Mass activities of Ni/GD, Fe/GD, and Pt/C (inset: mass activities obtained at overpotentials of 0.05 and 0.20 V). Reproduced with permission from Ref. [140]. Copyright 2018, Nature Publishing Group. (g) Schematic illustration of the synthesis of Co-SAS/HOPNC. (h) TEM and (i, j) AC HAADF-STEM images of the Co-SAS/HOPNC. Isolated single Co atoms are marked with light-yellow circles. (k) Fourier transforms of EXAFS curves of Co-SAS/HOPNC, CoO, Co_3O_4, and Co foil at Co K edge. (l) The corresponding EXAFS fitting curves of Co-SAS/HOPNC. Inset: schematic model of Co-SAS/HOPNC: Co (orange), N (blue), and C (gray). (m) HER LSV curves of the samples. Reproduced with permission from Ref. [144]. Copyright 2018, National Academy of Sciences.

I SASCs

Zhao *et al.* [147] prepared a Ni-I precursor in a vacuum-sealed ampoule; the sample underwent pyrolysis in vacuum, and cyclic voltammetric activation in KOH solutions, yielding a single-atom Ni-I catalyst (denoted as SANI-I). Most I atoms in the Ni-I precursor were replaced by oxygen atoms and hydroxide anions during the activation process. By HAADF-STEM and XAS characterizations, atomically dispersed I atoms were confirmed in the single-atom nickel iodide (SANi-I) catalyst. The SANi-I features a high structural stability, and high HER activity. The catalyst can deliver a current density of 100 mA cm^{-2} under an overpotential of 60 mV, better than those for Pt/C (61 mV) and A-Ni-OH (285 mV). The team investigated the HER mechanism using *in situ* Raman spectroscopy, and found that the Ni atoms adjacent to single I atoms can promote the formation of I-H_{ads} intermediates and thus accelerate the dissociation of adsorbed water molecules. This report uncovers new opportunities for non-metal-based SASCs in the field of energy conversion.

STRUCTURE-ACTIVITY RELATIONSHIP OF SASCs IN HER

Size effect

The size of catalyst is one of the key factors that influence the activity. By downsizing the catalytic entities, the atom utilization efficiency can be effectively elevated. For instance, Cheng *et al.* [148] employed N-doped graphene as support, and thereupon loaded a series of Pt catalysts with varying sizes *via* atomic layer deposition (ALD). By precisely controlling the ALD cycles, the size of Pt species can vary from single atoms, sub-nanometer clusters, to nanosized particles (Fig. 11a–b). The single Pt atoms and Pt clusters display exceptionally high activities (with a mass activity 37 times as high as that for commercial 20% Pt/C) and stabilities in 0.5 mol L^{-1} H_2SO_4 (Fig. 11c).

Coordination effect

The in-depth understanding of the structure-activity relationship between the coordination environments in SACs and their catalytic performances would be of guidance for the development and application of new, advanced SACs. For instance, Yin *et al.* [149] judiciously exploited the coordination affinity between C≡C bonds in graphdiyne support and Pt atoms, and successfully constructed two Pt-based SACs that feature different coordination environments (Fig. 11d and e). They found that the four-coordinated C_2-Pt-Cl_2 site has more unoccupied 5d orbitals, which is beneficial to the HER process. The catalyst with four-coordinated sites displays a superior HER mass activity and stability in 0.5 mol L^{-1} H_2SO_4, with its mass activity 3.3 and 26.9 times as high as

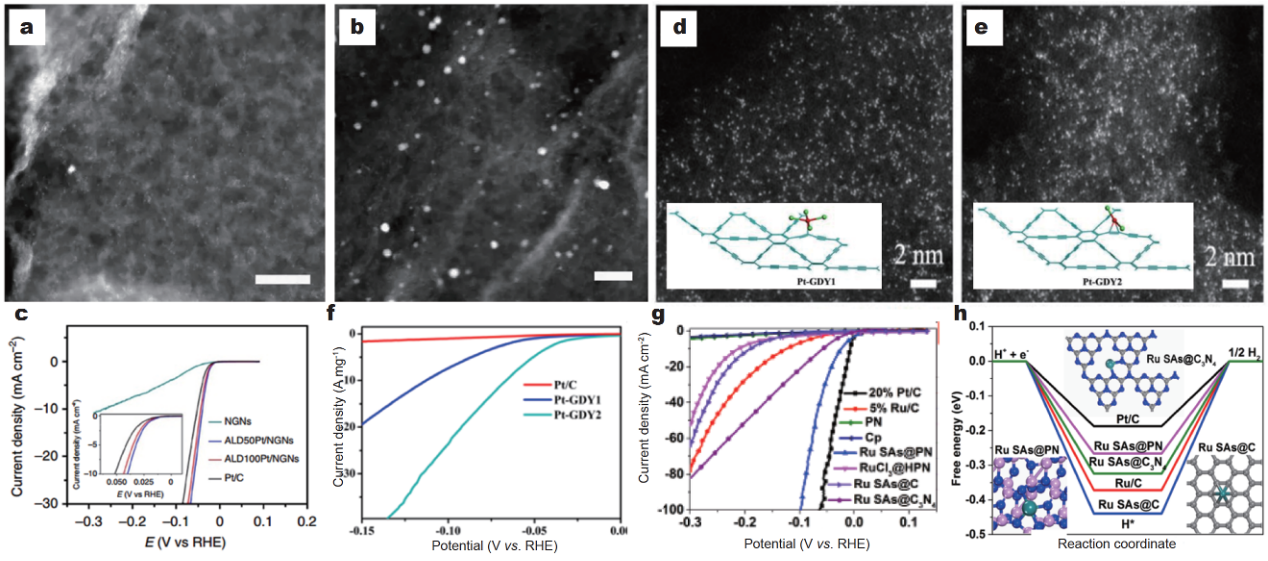

Figure 11 HAADF-STEM images of Pt/NGNs samples with (a) 50 and (b) 100 ALD cycles. Scale bars, 10 nm. (c) The HER LSV curves for Pt/NGNs and Pt/C catalysts in 0.5 mol L^{-1} H_2SO_4. The inset shows the enlarged curves at the onset potential region of the HER for the different catalysts. Reproduced with permission from Ref. [148]. Copyright 2016, Nature Publishing Group. AC-HAADF-STEM images for Pt-GDY1 (d) and Pt-GDY2 (e). Insets show the corresponding configuration. (f) The LSV curves for Pt-GDY1, Pt-GDY2 and Pt/C in 0.5 mol L^{-1} H_2SO_4. Adapted with permission from Ref. [149]. Copyright 2018, Wiley-VCH Verlag GmbH & Co. (g) The HER LSV curves of the catalysts. (h) The calculated free energy diagram for HER. Adapted with permission from Ref. [132]. Copyright 2018, Wiley-VCH Verlag GmbH & Co.

those for the catalyst with five-coordinated C-Pt-Cl_4 sites (Fig. 11f) and commercial Pt/C, respectively.

Support effect

As is well known, the role of support in catalysis is not merely to provide a large specific surface area, but more importantly, to help optimize the local geometric/electronic structures of metal species. For SACs, the support effect becomes more prominent. For instance, Yang *et al.* [132] compared single Ru atoms anchored on different supports, including PN imide nanotubes, commercial XC-72 conductive carbon black and C_3N_4. They found that the single Ru atoms on PN nanotubes give an overpotential as low as 24 mV at 10 mA cm^{-2}, only 14 mV higher than that for commercial Pt/C. By contrast, the Ru atoms anchored on XC-72 and C_3N_4 show 191 and 58 mV, respectively (Fig. 11g). The catalyst with PN support has a faster kinetics, with a Tafel slope of 38 mV dec^{-1}, lower than those for XC-72 (122 mV dec^{-1}) and C_3N_4 (125 mV dec^{-1}). Compared with carbon and C_3N_4 support, the ΔG_{H^*} of the Ru SAs on PN is much closer to 0, thus improving the HER performance (Fig. 11h). These results confirm that support effect plays a major role in Ru-based SACs for HER.

THE DEVELOPMENT TRENDS AND FACED CHALLENGES OF CATALYSTS FOR ELECTROCHEMICAL HER

Considering the research processes thus far, SASCs generally display high economicalness by virtue of the uniform active sites and maximized atomic utilization efficiency. Currently, the research on SASCs catering to HER is still in its infancy. Noble-metal-based SASCs have demonstrated activities and stabilities superior to those for commercial Pt/C, and also feature lower metal loadings and much reduced expenses. Despite the great promises of SACs, the bottlenecks in preparation are still limiting their applications. A major goal in this regard is to achieve the mass production of SASCs based on noble metals. For HER catalysts based on non-noble metals, their activities now can be comparable to that for commercial Pt/C; one of the future tasks is to develop general preparation methods that allow for large-scale production with high loadings, so as to achieve the replacement of noble metals.

For hydrogen production *via* electrochemical water splitting, it should be firstly noted that, although the reaction can be run at all pH values, the neutral pH condition is generally preferred. Second, most of the currently available techniques require pure water as reactant, whereas resources from other waterbodies (such as sea water, and industrial wastewater) received much less attention, primarily because the impurities in these waters can lead to side reactions and corrosion of the electrodes. Third, electrochemical water splitting, from the perspectives of both fundamental and application, has to overcome the issues of activity and stability under high current densities typical in industry, and relevant tests need to be run at a current density at least 500 or 1000 mA cm^{-2} for long terms. Last but not least, the electrochemical device for water splitting can be coupled with other systems, allowing for rich opportunities in, for example, sunlight-powered water splitting, coordinated HER and chlorine evolution reaction for chloralkali process, coordinated production of hydrogen and sulfur. Therefore, developing SACs with high activity, high selectivity, high stability and low cost for HER is the key to further elevating the catalytic efficiency.

SUMMARY AND PROSPECTS

In this review, we systematically summarized the research progresses regarding HER-oriented nanocatalysts, discussed the structure-activity relationship, and interpreted their high activities from an atomistic perspective; we also overviewed the design, preparation and applications of a variety of HER-oriented SASCs, as well as the structure-activity relationship at the atomic level, and discussed the future directions for the development of high-performance SASCs for HER. At the current stage, the research on SASCs is still at its infancy, and there exist a number of challenges in the development and application of SASCs catering to HER. Firstly, in regard to preparation, the cost of preparing SASCs has to be lowered; the carbon-supported SASCs thus far are mostly obtained *via* pyrolysis, and more facile preparation strategies are still in need (for example, preparing the catalysts directly from bulk metals). Secondly, powerful *in situ* characterization techniques are still in urgent demand (such as TEM, environmental AC-HAADF-STEM, XAS, Mössbauer spectroscopy), as these techniques enable *in situ* monitoring of the reaction processes, identification of the real active sites, and help deepen our understanding of the structure-activity relationship at the atomic level.

Received 11 November 2019; accepted 28 December 2019; published online 28 February 2020

1 Turner JA. Sustainable hydrogen production. Science, 2004, 305: 972–974
2 Zheng Y, Jiao Y, Qiao SZ. Engineering of carbon-based electrocatalysts for emerging energy conversion: From fundamentality

to functionality. Adv Mater, 2015, 27: 5372–5378
3 Shi Y, Zhang B. Recent advances in transition metal phosphide nanomaterials: Synthesis and applications in hydrogen evolution reaction. Chem Soc Rev, 2016, 45: 1529–1541
4 Yi JD, Liu TT, Huang YB, *et al.* Solid-state synthesis of MoS_2 nanorod from molybdenum-organic framework for efficient hydrogen evolution reaction. Sci China Mater, 2019, 62: 965–972
5 Cao Z, Chen Q, Zhang J, *et al.* Platinum-nickel alloy excavated nano-multipods with hexagonal close-packed structure and superior activity towards hydrogen evolution reaction. Nat Commun, 2017, 8: 15131–15137
6 Zou X, Zhang Y. Noble metal-free hydrogen evolution catalysts for water splitting. Chem Soc Rev, 2015, 44: 5148–5180
7 Zeng M, Li Y. Recent advances in heterogeneous electrocatalysts for the hydrogen evolution reaction. J Mater Chem A, 2015, 3: 14942–14962
8 Chen J, Lim B, Lee EP, *et al.* Shape-controlled synthesis of platinum nanocrystals for catalytic and electrocatalytic applications. Nano Today, 2009, 4: 81–95
9 Li Y, Zhang H, Xu T, *et al.* Under-water superaerophobic pine-shaped Pt nanoarray electrode for ultrahigh-performance hydrogen evolution. Adv Funct Mater, 2015, 25: 1737–1744
10 Bai S, Wang C, Deng M, *et al.* Surface polarization matters: Enhancing the hydrogen-evolution reaction by shrinking Pt shells in Pt-Pd-graphene stack structures. Angew Chem Int Ed, 2014, 53: 12120–12124
11 Esposito DV, Chen JG. Monolayer platinum supported on tungsten carbides as low-cost electrocatalysts: Opportunities and limitations. Energy Environ Sci, 2011, 4: 3900–3912
12 Xing Z, Han C, Wang D, *et al.* Ultrafine Pt nanoparticle-decorated $Co(OH)_2$ nanosheet arrays with enhanced catalytic activity toward hydrogen evolution. ACS Catal, 2017, 7: 7131–7135
13 Xie L, Ren X, Liu Q, *et al.* A $Ni(OH)_2$-PtO_2 hybrid nanosheet array with ultralow Pt loading toward efficient and durable alkaline hydrogen evolution. J Mater Chem A, 2018, 6: 1967–1970
14 Tiwari JN, Sultan S, Myung CW, *et al.* Multicomponent electrocatalyst with ultralow Pt loading and high hydrogen evolution activity. Nat Energy, 2018, 3: 773–782
15 Yang H, Wang C, Hu F, *et al.* Atomic-scale Pt clusters decorated on porous α-$Ni(OH)_2$ nanowires as highly efficient electrocatalyst for hydrogen evolution reaction. Sci China Mater, 2017, 60: 1121–1128
16 Wang S, Gao X, Hang X, *et al.* Ultrafine Pt nanoclusters confined in a calixarene-based $\{Ni_{24}\}$ coordination cage for high-efficient hydrogen evolution reaction. J Am Chem Soc, 2016, 138: 16236–16239
17 Chao T, Luo X, Chen W, *et al.* Atomically dispersed copper-platinum dual sites alloyed with palladium nanorings catalyze the hydrogen evolution reaction. Angew Chem Int Ed, 2017, 56: 16047–16051
18 Kerkeni S, Lamy-Pitara E, Barbier J. Copper-platinum catalysts prepared and characterized by electrochemical methods for the reduction of nitrate and nitrite. Catal Today, 2002, 75: 35–42
19 Zhong X, Wang L, Zhuang Z, *et al.* Double nanoporous structure with nanoporous PtFe embedded in graphene nanopores: Highly efficient bifunctional electrocatalysts for hydrogen evolution and oxygen reduction. Adv Mater Interfaces, 2017, 4: 1601029
20 Yang TT, Zhu H, Wan M, *et al.* Highly efficient and durable PtCo alloy nanoparticles encapsulated in carbon nanofibers for electrochemical hydrogen generation. Chem Commun, 2016, 52: 990–993
21 Zhang Z, Liu G, Cui X, *et al.* Crystal phase and architecture engineering of lotus-thalamus-shaped Pt-Ni anisotropic superstructures for highly efficient electrochemical hydrogen evolution. Adv Mater, 2018, 30: 1801741
22 Oh A, Sa YJ, Hwang H, *et al.* Rational design of Pt-Ni-Co ternary alloy nanoframe crystals as highly efficient catalysts toward the alkaline hydrogen evolution reaction. Nanoscale, 2016, 8: 16379–16386
23 Shen Y, Lua AC, Xi J, *et al.* Ternary platinum-copper-nickel nanoparticles anchored to hierarchical carbon supports as free-standing hydrogen evolution electrodes. ACS Appl Mater Interfaces, 2016, 8: 3464–3472
24 Gong M, Zhou W, Tsai MC, *et al.* Nanoscale nickel oxide/nickel heterostructures for active hydrogen evolution electrocatalysis. Nat Commun, 2014, 5: 4695
25 Deng J, Ren P, Deng D, *et al.* Highly active and durable non-precious-metal catalysts encapsulated in carbon nanotubes for hydrogen evolution reaction. Energy Environ Sci, 2014, 7: 1919–1923
26 Deng J, Ren P, Deng D, *et al.* Enhanced electron penetration through an ultrathin graphene layer for highly efficient catalysis of the hydrogen evolution reaction. Angew Chem Int Ed, 2015, 54: 2100–2104
27 Tavakkoli M, Kallio T, Reynaud O, *et al.* Single-shell carbon-encapsulated iron nanoparticles: Synthesis and high electrocatalytic activity for hydrogen evolution reaction. Angew Chem Int Ed, 2015, 54: 4535–4538
28 Nørskov JK, Bligaard T, Logadottir A, *et al.* Trends in the exchange current for hydrogen evolution. J Electrochem Soc, 2005, 152: J23
29 Liu P, Rodriguez JA. Catalysts for hydrogen evolution from the [NiFe] hydrogenase to the $Ni_2P(001)$ surface: The importance of ensemble effect. J Am Chem Soc, 2005, 127: 14871–14878
30 Popczun EJ, McKone JR, Read CG, *et al.* Nanostructured nickel phosphide as an electrocatalyst for the hydrogen evolution reaction. J Am Chem Soc, 2013, 135: 9267–9270
31 Xu Y, Wu R, Zhang J, *et al.* Anion-exchange synthesis of nanoporous FeP nanosheets as electrocatalysts for hydrogen evolution reaction. Chem Commun, 2013, 49: 6656–6658
32 Lu S, Zhuang Z. Electrocatalysts for hydrogen oxidation and evolution reactions. Sci China Mater, 2016, 59: 217–238
33 Zhao X, Luo D, Wang Y, *et al.* Reduced graphene oxide-supported CoP nanocrystals confined in porous nitrogen-doped carbon nanowire for highly enhanced lithium/sodium storage and hydrogen evolution reaction. Nano Res, 2019, 12: 2872–2880
34 Pan Y, Sun K, Liu S, *et al.* Core-shell ZIF-8@ZIF-67-derived CoP nanoparticle-embedded N-doped carbon nanotube hollow polyhedron for efficient overall water splitting. J Am Chem Soc, 2018, 140: 2610–2618
35 Zhao D, Sun K, Cheong WC, *et al.* Synergistically interactive pyridinic-N-MoP sites: Identified active centers for enhanced hydrogen evolution in alkaline solution. Angew Chem, 2019, : ange.201908760
36 Xiao P, Sk MA, Thia L, *et al.* Molybdenum phosphide as an efficient electrocatalyst for the hydrogen evolution reaction. Energy Environ Sci, 2014, 7: 2624–2629
37 Hao J, Yang W, Zhang Z, *et al.* Metal-organic frameworks derived $Co_xFe_{1-x}P$ nanocubes for electrochemical hydrogen evolution. Nanoscale, 2015, 7: 11055–11062

38 Li Y, Zhang H, Jiang M, *et al.* Ternary NiCoP nanosheet arrays: An excellent bifunctional catalyst for alkaline overall water splitting. Nano Res, 2016, 9: 2251–2259
39 Tang C, Gan L, Zhang R, *et al.* Ternary $Fe_xCo_{1-x}P$ nanowire array as a robust hydrogen evolution reaction electrocatalyst with Pt-like activity: Experimental and theoretical insight. Nano Lett, 2016, 16: 6617–6621
40 Li Y, Zhang H, Jiang M, *et al.* 3D self-supported Fe-doped Ni_2P nanosheet arrays as bifunctional catalysts for overall water splitting. Adv Funct Mater, 2017, 27: 1702513
41 Liang X, Zhang D, Wu Z, *et al.* The Fe-promoted MoP catalyst with high activity for water splitting. Appl Catal A-General, 2016, 524: 134–138
42 Li J, Yan M, Zhou X, *et al.* Mechanistic insights on ternary $Ni_{2-x}Co_xP$ for hydrogen evolution and their hybrids with graphene as highly efficient and robust catalysts for overall water splitting. Adv Funct Mater, 2016, 26: 6785–6796
43 Man HW, Tsang CS, Li MMJ, *et al.* Transition metal-doped nickel phosphide nanoparticles as electro- and photocatalysts for hydrogen generation reactions. Appl Catal B-Environ, 2019, 242: 186–193
44 Zhang LF, Ke X, Ou G, *et al.* Defective MoS_2 electrocatalyst for highly efficient hydrogen evolution through a simple ball-milling method. Sci China Mater, 2017, 60: 849–856
45 Di Giovanni C, Wang WA, Nowak S, *et al.* Bioinspired iron sulfide nanoparticles for cheap and long-lived electrocatalytic molecular hydrogen evolution in neutral water. ACS Catal, 2014, 4: 681–687
46 Kong D, Cha JJ, Wang H, *et al.* First-row transition metal dichalcogenide catalysts for hydrogen evolution reaction. Energy Environ Sci, 2013, 6: 3553
47 Faber MS, Dziedzic R, Lukowski MA, *et al.* High-performance electrocatalysis using metallic cobalt pyrite (CoS_2) micro- and nanostructures. J Am Chem Soc, 2014, 136: 10053–10061
48 Peng S, Li L, Han X, *et al.* Cobalt sulfide nanosheet/graphene/carbon nanotube nanocomposites as flexible electrodes for hydrogen evolution. Angew Chem, 2014, 126: 12802–12807
49 Tang C, Pu Z, Liu Q, *et al.* NiS_2 nanosheets array grown on carbon cloth as an efficient 3D hydrogen evolution cathode. Electrochim Acta, 2015, 153: 508–514
50 Voiry D, Yamaguchi H, Li J, *et al.* Enhanced catalytic activity in strained chemically exfoliated WS_2 nanosheets for hydrogen evolution. Nat Mater, 2013, 12: 850–855
51 Zhao X, Ma X, Sun J, *et al.* Enhanced catalytic activities of surfactant-assisted exfoliated WS_2 nanodots for hydrogen evolution. ACS Nano, 2016, 10: 2159–2166
52 Xu S, Li D, Wu P. One-pot, facile, and versatile synthesis of monolayer MoS_2/WS_2 quantum dots as bioimaging probes and efficient electrocatalysts for hydrogen evolution reaction. Adv Funct Mater, 2015, 25: 1127–1136
53 Duan J, Chen S, Chambers BA, *et al.* 3D WS_2 nanolayers@heteroatom-doped graphene films as hydrogen evolution catalyst electrodes. Adv Mater, 2015, 27: 4234–4241
54 Tributsch H, Bennett JC. Electrochemistry and photochemistry of MoS_2 layer crystals. I. J Electroanal Chem Interfacial Electrochem, 1977, 81: 97–111
55 Hinnemann B, Moses PG, Bonde J, *et al.* Biomimetic hydrogen evolution: MoS_2 nanoparticles as catalyst for hydrogen evolution. J Am Chem Soc, 2005, 127: 5308–5309
56 Jaramillo TF, Jørgensen KP, Bonde J, *et al.* Identification of active edge sites for electrochemical H_2 evolution from MoS_2 nanocatalysts. Science, 2007, 317: 100–102
57 Liu D, Xu W, Liu Q, *et al.* Unsaturated-sulfur-rich MoS_2 nanosheets decorated on free-standing SWNT film: Synthesis, characterization and electrocatalytic application. Nano Res, 2016, 9: 2079–2087
58 Kong D, Wang H, Cha JJ, *et al.* Synthesis of MoS_2 and $MoSe_2$ films with vertically aligned layers. Nano Lett, 2013, 13: 1341–1347
59 Kibsgaard J, Chen Z, Reinecke BN, *et al.* Engineering the surface structure of MoS_2 to preferentially expose active edge sites for electrocatalysis. Nat Mater, 2012, 11: 963–969
60 Wang Z, Li Q, Xu H, *et al.* Controllable etching of MoS_2 basal planes for enhanced hydrogen evolution through the formation of active edge sites. Nano Energy, 2018, 49: 634–643
61 Li H, Tsai C, Koh AL, *et al.* Activating and optimizing MoS_2 basal planes for hydrogen evolution through the formation of strained sulphur vacancies. Nat Mater, 2016, 15: 48–53
62 Li H, Du M, Mleczko MJ, *et al.* Kinetic study of hydrogen evolution reaction over strained MoS_2 with sulfur vacancies using scanning electrochemical microscopy. J Am Chem Soc, 2016, 138: 5123–5129
63 Tsai C, Li H, Park S, *et al.* Electrochemical generation of sulfur vacancies in the basal plane of MoS_2 for hydrogen evolution. Nat Commun, 2017, 8: 15113
64 Li G, Zhang D, Qiao Q, *et al.* All the catalytic active sites of MoS_2 for hydrogen evolution. J Am Chem Soc, 2016, 138: 16632–16638
65 Zhu J, Wang ZC, Dai H, *et al.* Boundary activated hydrogen evolution reaction on monolayer MoS_2. Nat Commun, 2019, 10: 1348
66 Gao MR, Lin ZY, Zhuang TT, *et al.* Mixed-solution synthesis of sea urchin-like NiSe nanofiber assemblies as economical Pt-free catalysts for electrochemical H_2 production. J Mater Chem, 2012, 22: 13662
67 Zhou H, Yu F, Liu Y, *et al.* Outstanding hydrogen evolution reaction catalyzed by porous nickel diselenide electrocatalysts. Energy Environ Sci, 2017, 10: 1487–1492
68 Kong D, Wang H, Lu Z, *et al.* $CoSe_2$ nanoparticles grown on carbon fiber paper: An efficient and stable electrocatalyst for hydrogen evolution reaction. J Am Chem Soc, 2014, 136: 4897–4900
69 Tsai C, Chan K, Abild-Pedersen F, *et al.* Active edge sites in $MoSe_2$ and WSe_2 catalysts for the hydrogen evolution reaction: A density functional study. Phys Chem Chem Phys, 2014, 16: 13156–13164
70 Liu Z, Li N, Zhao H, *et al.* Colloidally synthesized $MoSe_2$/graphene hybrid nanostructures as efficient electrocatalysts for hydrogen evolution. J Mater Chem A, 2015, 3: 19706–19710
71 Tang H, Dou K, Kaun CC, *et al.* $MoSe_2$ nanosheets and their graphene hybrids: Synthesis, characterization and hydrogen evolution reaction studies. J Mater Chem A, 2014, 2: 360–364
72 Yin Y, Zhang Y, Gao T, *et al.* Synergistic phase and disorder engineering in 1T-$MoSe_2$ nanosheets for enhanced hydrogen-evolution reaction. Adv Mater, 2017, 29: 1700311
73 Peng X, Hu L, Wang L, *et al.* Vanadium carbide nanoparticles encapsulated in graphitic carbon network nanosheets: A high-efficiency electrocatalyst for hydrogen evolution reaction. Nano Energy, 2016, 26: 603–609
74 Xiong W, Guo Q, Guo Z, *et al.* Atomic layer deposition of nickel carbide for supercapacitors and electrocatalytic hydrogen evolu-

tion. J Mater Chem A, 2018, 6: 4297–4304
75 Meyer S, Nikiforov AV, Petrushina IM, *et al.* Transition metal carbides (WC, Mo_2C, TaC, NbC) as potential electrocatalysts for the hydrogen evolution reaction (HER) at medium temperatures. Int J Hydrogen Energy, 2015, 40: 2905–2911
76 Levy RB, Boudart M. Platinum-like behavior of tungsten carbide in surface catalysis. Science, 1973, 181: 547–549
77 Bennett LH, Cuthill JR, McAlister AJ, *et al.* Electronic structure and catalytic behavior of tungsten carbide. Science, 1974, 184: 563–565
78 Xu YT, Xiao X, Ye ZM, *et al.* Cage-confinement pyrolysis route to ultrasmall tungsten carbide nanoparticles for efficient electrocatalytic hydrogen evolution. J Am Chem Soc, 2017, 139: 5285–5288
79 Kim SK, Qiu Y, Zhang YJ, *et al.* Nanocomposites of transition-metal carbides on reduced graphite oxide as catalysts for the hydrogen evolution reaction. Appl Catal B-Environ, 2018, 235: 36–44
80 Ma R, Zhou Y, Chen Y, *et al.* Ultrafine molybdenum carbide nanoparticles composited with carbon as a highly active hydrogen-evolution electrocatalyst. Angew Chem Int Ed, 2015, 54: 14723–14727
81 Ko YJ, Cho JM, Kim I, *et al.* Tungsten carbide nanowalls as electrocatalyst for hydrogen evolution reaction: New approach to durability issue. Appl Catal B-Environ, 2017, 203: 684–691
82 Wu HB, Xia BY, Yu L, *et al.* Porous molybdenum carbide nano-octahedrons synthesized *via* confined carburization in metal-organic frameworks for efficient hydrogen production. Nat Commun, 2015, 6: 6512
83 Humagain G, MacDougal K, MacInnis J, *et al.* Highly efficient, biochar-derived molybdenum carbide hydrogen evolution electrocatalyst. Adv Energy Mater, 2018, 8: 1801461
84 Ren B, Li D, Jin Q, *et al.* A self-supported porous WN nanowire array: An efficient 3D electrocatalyst for the hydrogen evolution reaction. J Mater Chem A, 2017, 5: 19072–19078
85 Xing Z, Li Q, Wang D, *et al.* Self-supported nickel nitride as an efficient high-performance three-dimensional cathode for the alkaline hydrogen evolution reaction. Electrochim Acta, 2016, 191: 841–845
86 You B, Liu X, Hu G, *et al.* Universal surface engineering of transition metals for superior electrocatalytic hydrogen evolution in neutral water. J Am Chem Soc, 2017, 139: 12283–12290
87 Xie J, Li S, Zhang X, *et al.* Atomically-thin molybdenum nitride nanosheets with exposed active surface sites for efficient hydrogen evolution. Chem Sci, 2014, 5: 4615–4620
88 Liang HW, Brüller S, Dong R, *et al.* Molecular metal-N_x centres in porous carbon for electrocatalytic hydrogen evolution. Nat Commun, 2015, 6: 7992
89 Yu F, Zhou H, Zhu Z, *et al.* Three-dimensional nanoporous iron nitride film as an efficient electrocatalyst for water oxidation. ACS Catal, 2017, 7: 2052–2057
90 Yu L, Song S, McElhenny B, *et al.* A universal synthesis strategy to make metal nitride electrocatalysts for hydrogen evolution reaction. J Mater Chem A, 2019, 7: 19728–19732
91 Han Y, Yue X, Jin Y, *et al.* Hydrogen evolution reaction in acidic media on single-crystalline titanium nitride nanowires as an efficient non-noble metal electrocatalyst. J Mater Chem A, 2016, 4: 3673–3677
92 Zhu Y, Chen G, Zhong Y, *et al.* Rationally designed hierarchically structured tungsten nitride and nitrogen-rich graphene-like carbon nanocomposite as efficient hydrogen evolution electrocatalyst. Adv Sci, 2018, 5: 1700603
93 Los P, Lasia A. Electrocatalytic properties of amorphous nickel boride electrodes for hydrogen evolution reaction in alkaline solution. J Electroanal Chem, 1992, 333: 115–125
94 Albert B, Hillebrecht H. Boron: Elementary challenge for experimenters and theoreticians. Angew Chem Int Ed, 2009, 48: 8640–8668
95 Masa J, Weide P, Peeters D, *et al.* Amorphous cobalt boride (Co_2B) as a highly efficient nonprecious catalyst for electrochemical water splitting: Oxygen and hydrogen evolution. Adv Energy Mater, 2016, 6: 1502313
96 Lu W, Liu T, Xie L, *et al. In situ* derived Co-B nanoarray: A high-efficiency and durable 3D bifunctional electrocatalyst for overall alkaline water splitting. Small, 2017, 13: 1700805
97 Zhang P, Wang M, Yang Y, *et al.* Electroless plated Ni-B films as highly active electrocatalysts for hydrogen production from water over a wide pH range. Nano Energy, 2016, 19: 98–107
98 Vrubel H, Hu X. Molybdenum boride and carbide catalyze hydrogen evolution in both acidic and basic solutions. Angew Chem Int Ed, 2012, 51: 12703–12706
99 Park H, Encinas A, Scheifers JP, *et al.* Boron-dependency of molybdenum boride electrocatalysts for the hydrogen evolution reaction. Angew Chem Int Ed, 2017, 56: 5575–5578
100 Gupta S, Patel N, Fernandes R, *et al.* Co-Ni-B nanocatalyst for efficient hydrogen evolution reaction in wide pH range. Appl Catal B-Environ, 2016, 192: 126–133
101 Xu N, Cao G, Chen Z, *et al.* Cobalt nickel boride as an active electrocatalyst for water splitting. J Mater Chem A, 2017, 5: 12379–12384
102 Cao S, Tao FF, Tang Y, *et al.* Size- and shape-dependent catalytic performances of oxidation and reduction reactions on nanocatalysts. Chem Soc Rev, 2016, 45: 4747–4765
103 Pan Y, Liu Y, Zhao J, *et al.* Monodispersed nickel phosphide nanocrystals with different phases: Synthesis, characterization and electrocatalytic properties for hydrogen evolution. J Mater Chem A, 2015, 3: 1656–1665
104 Pan Y, Lin Y, Chen Y, *et al.* Cobalt phosphide-based electrocatalysts: Synthesis and phase catalytic activity comparison for hydrogen evolution. J Mater Chem A, 2016, 4: 4745–4754
105 Callejas JF, Read CG, Popczun EJ, *et al.* Nanostructured Co_2P electrocatalyst for the hydrogen evolution reaction and direct comparison with morphologically equivalent CoP. Chem Mater, 2015, 27: 3769–3774
106 Yin Y, Han J, Zhang Y, *et al.* Contributions of phase, sulfur vacancies, and edges to the hydrogen evolution reaction catalytic activity of porous molybdenum disulfide nanosheets. J Am Chem Soc, 2016, 138: 7965–7972
107 Lukowski MA, Daniel AS, Meng F, *et al.* Enhanced hydrogen evolution catalysis from chemically exfoliated metallic MoS_2 nanosheets. J Am Chem Soc, 2013, 135: 10274–10277
108 Sun K, Liu Y, Pan Y, *et al.* Targeted bottom-up synthesis of 1T-phase MoS_2 arrays with high electrocatalytic hydrogen evolution activity by simultaneous structure and morphology engineering. Nano Res, 2018, 11: 4368–4379
109 Yu X, Yu ZY, Zhang XL, *et al.* "Superaerophobic" nickel phosphide nanoarray catalyst for efficient hydrogen evolution at ultrahigh current densities. J Am Chem Soc, 2019, 141: 7537–7543
110 Wang J, Yang Q, Wang M, *et al.* Rose petals with a novel and steady air bubble pinning effect in aqueous media. Soft Matter,

2012, 8: 2261–2266
111 Lu Z, Zhu W, Yu X, *et al.* Ultrahigh hydrogen evolution performance of under-water "Superaerophobic" MoS_2 nanostructured electrodes. Adv Mater, 2014, 26: 2683–2687
112 Zhang J, Sui R, Xue Y, *et al.* Direct synthesis of parallel doped N-MoP/N-CNT as highly active hydrogen evolution reaction catalyst. Sci China Mater, 2019, 62: 690–698
113 Qu G, Wu T, Yu Y, *et al.* Rational design of phosphorus-doped cobalt sulfides electrocatalysts for hydrogen evolution. Nano Res, 2019, 12: 2960–2965
114 Wang DY, Gong M, Chou HL, *et al.* Highly active and stable hybrid catalyst of cobalt-doped FeS_2 nanosheets-carbon nanotubes for hydrogen evolution reaction. J Am Chem Soc, 2015, 137: 1587–1592
115 Hou Y, Qiu M, Zhang T, *et al.* Ternary porous cobalt phosphoselenide nanosheets: An efficient electrocatalyst for electrocatalytic and photoelectrochemical water splitting. Adv Mater, 2017, 29: 1701589
116 Kibsgaard J, Jaramillo TF. Molybdenum phosphosulfide: An active, acid-stable, earth-abundant catalyst for the hydrogen evolution reaction. Angew Chem Int Ed, 2014, 53: 14433–14437
117 Cabán-Acevedo M, Stone ML, Schmidt JR, *et al.* Efficient hydrogen evolution catalysis using ternary pyrite-type cobalt phosphosulphide. Nat Mater, 2015, 14: 1245–1251
118 Hong W, Jian C, Wang G, *et al.* Self-supported nanoporous cobalt phosphosulfate electrodes for efficient hydrogen evolution reaction. Appl Catal B-Environ, 2019, 251: 213–219
119 Chen Z, Song Y, Cai J, *et al.* Tailoring the d-band centers enables Co_4N nanosheets to be highly active for hydrogen evolution catalysis. Angew Chem Int Ed, 2018, 57: 5076–5080
120 Pan Y, Sun K, Lin Y, *et al.* Electronic structure and d-band center control engineering over M-doped CoP (M = Ni, Mn, Fe) hollow polyhedron frames for boosting hydrogen production. Nano Energy, 2019, 56: 411–419
121 Tan C, Chen J, Wu XJ, *et al.* Epitaxial growth of hybrid nanostructures. Nat Rev Mater, 2018, 3: 17089
122 Zhao G, Rui K, Dou SX, *et al.* Heterostructures for electrochemical hydrogen evolution reaction: A review. Adv Funct Mater, 2018, 28: 1803291
123 Lin Y, Sun K, Liu S, *et al.* Construction of CoP/NiCoP nanotadpoles heterojunction interface for wide pH hydrogen evolution electrocatalysis and supercapacitor. Adv Energy Mater, 2019, 9: 1901213
124 Lin Y, Pan Y, Liu S, *et al.* Construction of multi-dimensional core/shell Ni/NiCoP nano-heterojunction for efficient electrocatalytic water splitting. Appl Catal B-Environ, 2019, 259: 118039
125 Wang P, Zhang X, Zhang J, *et al.* Precise tuning in platinum-nickel/nickel sulfide interface nanowires for synergistic hydrogen evolution catalysis. Nat Commun, 2017, 8: 14580
126 Liu D, Li X, Chen S, *et al.* Atomically dispersed platinum supported on curved carbon supports for efficient electrocatalytic hydrogen evolution. Nat Energy, 2019, 4: 512–518
127 Zhang J, Zhao Y, Guo X, *et al.* Single platinum atoms immobilized on an MXene as an efficient catalyst for the hydrogen evolution reaction. Nat Catal, 2018, 1: 985–992
128 Ye S, Luo F, Zhang Q, *et al.* Highly stable single Pt atomic sites anchored on aniline-stacked graphene for hydrogen evolution reaction. Energy Environ Sci, 2019, 12: 1000–1007
129 Zhang H, An P, Zhou W, *et al.* Dynamic traction of lattice-confined platinum atoms into mesoporous carbon matrix for hydrogen evolution reaction. Sci Adv, 2018, 4: eaao6657
130 Zhang L, Han L, Liu H, *et al.* Potential-cycling synthesis of single platinum atoms for efficient hydrogen evolution in neutral media. Angew Chem Int Ed, 2017, 56: 13694–13698
131 Jiang K, Liu B, Luo M, *et al.* Single platinum atoms embedded in nanoporous cobalt selenide as electrocatalyst for accelerating hydrogen evolution reaction. Nat Commun, 2019, 10: 1743
132 Yang J, Chen B, Liu X, *et al.* Efficient and robust hydrogen evolution: Phosphorus nitride imide nanotubes as supports for anchoring single ruthenium sites. Angew Chem Int Ed, 2018, 57: 9495–9500
133 Ramalingam V, Varadhan P, Fu HC, *et al.* Heteroatom-mediated interactions between ruthenium single atoms and an MXene support for efficient hydrogen evolution. Adv Mater, 2019, 31: 1903841
134 Zhang L, Si R, Liu H, *et al.* Atomic layer deposited Pt-Ru dual-metal dimers and identifying their active sites for hydrogen evolution reaction. Nat Commun, 2019, 10: 4936
135 Lai W, Zhang L, Hua W, *et al.* General π-electron-assisted strategy for Ir, Pt, Ru, Pd, Fe, Ni single-atom electrocatalysts with bifunctional active sites for highly efficient water splitting. Angew Chem, 2019, 131: 11994–11999
136 Zhang L, Jia Y, Gao G, *et al.* Graphene defects trap atomic Ni species for hydrogen and oxygen evolution reactions. Chem, 2018, 4: 285–297
137 Li M, Duanmu K, Wan C, *et al.* Single-atom tailoring of platinum nanocatalysts for high-performance multifunctional electrocatalysis. Nat Catal, 2019, 2: 495–503
138 Zhang H, Yu L, Chen T, *et al.* Surface modulation of hierarchical MoS_2 nanosheets by Ni single atoms for enhanced electrocatalytic hydrogen evolution. Adv Funct Mater, 2018, 28: 1807086
139 Ling C, Shi L, Ouyang Y, *et al.* Nanosheet supported single-metal atom bifunctional catalyst for overall water splitting. Nano Lett, 2017, 17: 5133–5139
140 Xue Y, Huang B, Yi Y, *et al.* Anchoring zero valence single atoms of nickel and iron on graphdiyne for hydrogen evolution. Nat Commun, 2018, 9: 1460
141 Pan Y, Liu S, Sun K, *et al.* A bimetallic Zn/Fe polyphthalocyanine-derived single-atom Fe-N_4 catalytic site: A superior trifunctional catalyst for overall water splitting and Zn-air batteries. Angew Chem Int Ed, 2018, 57: 8614–8618
142 Fei H, Dong J, Arellano-Jiménez MJ, *et al.* Atomic cobalt on nitrogen-doped graphene for hydrogen generation. Nat Commun, 2015, 6: 8668
143 Fei H, Dong J, Wan C, *et al.* Microwave-assisted rapid synthesis of graphene-supported single atomic metals. Adv Mater, 2018, 30: 1802146
144 Sun T, Zhao S, Chen W, *et al.* Single-atomic cobalt sites embedded in hierarchically ordered porous nitrogen-doped carbon as a superior bifunctional electrocatalyst. Proc Natl Acad Sci USA, 2018, 115: 12692–12697
145 Chen W, Pei J, He CT, *et al.* Rational design of single molybdenum atoms anchored on N-doped carbon for effective hydrogen evolution reaction. Angew Chem Int Ed, 2017, 56: 16086–16090
146 Chen W, Pei J, He CT, *et al.* Single tungsten atoms supported on MOF-derived N-doped carbon for robust electrochemical hydrogen evolution. Adv Mater, 2018, 30: 1800396
147 Zhao Y, Ling T, Chen S, *et al.* Non-metal single-iodine-atom electrocatalysts for the hydrogen evolution reaction. Angew Chem Int Ed, 2019, 58: 12252–12257

148 Cheng N, Stambula S, Wang D, *et al.* Platinum single-atom and cluster catalysis of the hydrogen evolution reaction. Nat Commun, 2016, 7: 13638–13643
149 Yin XP, Wang HJ, Tang SF, *et al.* Engineering the coordination environment of single-atom platinum anchored on graphdiyne for optimizing electrocatalytic hydrogen evolution. Angew Chem Int Ed, 2018, 57: 9382–9386

Acknowledgements This work was supported by the National Key R&D Program of China (2016YFA0202801, 2017YFA0700101 and 2018YFA0702003), the National Natural Science Foundation of China (21925202, 21872076 and 21890383), Beijing Natural Science Foundation (JQ18007), the Fundamental Research Funds for the Central Universities (19CX02008A), the Petro China Innovation Foundation (2019D-5007-0401), Taishan Scholars Program of Shandong Province (tsqn201909065), and Tsinghua University Initiative Scientific Research Program.

Author contributions Pan Y and Chen C wrote the manuscript. Zhang C and Lin Y revised the manuscript. Liu Z and Wang M drew the figures. Chen C supervised the project, directed the research and established the final version of the manuscript. All authors participated in the general discussion.

Conflict of interest The authors declare no competing financial interests.

Yuan Pan received his PhD from the College of Chemical Engineering, China University of Petroleum (East China) in 2016. After postdoctoral work at Tsinghua University, he joined the College of Chemical Engineering at China University of Petroleum (East China) as an associate professor in 2019. His research interests focus on the design and synthesis of novel nanomaterials and single-atom materials for catalytic application.

Chen Chen received his BS degree from the Department of Chemistry, Beijing Institute of Technology in 2006, and his PhD degree from the Department of Chemistry, Tsinghua University in 2011. After postdoctoral work at Lawrence Berkeley National Laboratory, he joined the Department of Chemistry at Tsinghua University as an associate professor in 2015. His research interests focus on nanomaterials and catalysis.

析氢反应中电催化剂设计与构效关系：从纳米结构到单原子

潘原[1,2], 张超[2], 林燕[3], 刘智[1], 王敏敏[1], 陈晨[2*]

摘要 随着全球能源需求的增加和环境污染的加剧, 氢能作为一种新型的能源越来越受到广泛的关注. 高效催化剂的设计和开发是制氢研究中极具挑战性的难题. 催化剂的表界面组成与结构对其性能具有极其重要的影响, 如何科学地设计调控催化材料表界面结构来提高电催化析氢反应的活性和稳定性一直是催化领域研究的重点. 本综述针对电催化析氢体系中的多尺度催化剂设计合成为研究对象, 以纳米结构催化剂的设计及构效关系为出发点, 总结了目前针对电催化析氢反应的纳米催化剂的合成及构效关系的研究进展, 从原子尺度提出纳米催化剂高活性的起源. 结合目前报道的各种单原子催化剂的设计合成、在析氢反应中的应用及构效关系的研究, 讨论了设计定向单原子位点析氢催化剂的方向, 同时对电解水制氢催化剂的发展趋势和挑战进行了展望.

